Swiss J Geosci (2016) 109:309–328
DOI 10.1007/s00015-016-0234-3

Triassic magmatism on the transition from Variscan to Alpine cycles: evidence from U–Pb, Hf, and geochemistry of detrital minerals

Alejandro Beltrán-Triviño[1] · Wilfried Winkler[1] · Albrecht von Quadt[1] · Daniela Gallhofer[1]

Received: 26 June 2015 / Accepted: 2 November 2016 / Published online: 22 November 2016

Abstract New data on the U–Pb geochronology and Hf-isotopic composition of detrital zircons, along with the geochemistry of garnets, chromian spinel and feldspars from Permian and Triassic volcano-sedimentary sequences in the Southern and Eastern Alps reveal similarities in the nature and tectonomagmatic setting of the Early Permian and the Middle Triassic magmatic events. Detrital zircon U–Pb geochronology displays magmatic activity at 290–280 Ma (Early Permian) and at 245–235 Ma (Middle Triassic). The two-stage Hf-depleted mantle model ages obtained from Permian and Triassic zircons cluster around 1.7–1.6 and 1.3–0.8 Ga. Epsilon Hafnium analysis on dated detrital zircons suggests mixing of mantle and crustal components into the parental magmas of Permian and Triassic magmatism, the latter showing less crustal contribution. The composition of detrital feldspars from the Permian and Triassic volcaniclastic sandstones reveals provenance from intermediate to acidic igneous rocks. Garnet in Middle and Late Triassic beds suggests the incorporation of material comparable to the mafic rocks of the Ivrea-Verbano Zone into the parental melts of the Triassic magmatism. Chromian spinel in syn-magmatic Carnian sandstones indicates an origin associated with MORB-type peridotites and therefore, corroborates a mantle contribution to the Middle Triassic magmatism. The integration of detrital zircon U–Pb ages, Hf isotopes and composition of detrital minerals suggests that continuous lithospheric stretching at the transition from the post-Variscan to the Alpine orogenic cycle, with periods of strike-slip movements, presumably led to an asymmetrical continental rifting process, in which the Middle Triassic magmatic episode represents the earliest stage of the Alpine Tethys oceanic domain.

Keywords European Eastern and Southern Alps · Permian and Triassic magmatism · Detrital zircons U–Pb dating · Detrital zircons Hf-isotopes · Garnet geochemistry · Chromian spinel geochemistry · Feldspar geochemistry

1 Introduction

Intense Early Permian and Middle Triassic magmatic activity in the South-Alpine and Austroalpine palaeogeographic domains is evidenced by a widespread distribution of magmatic products in Permian and Triassic basins in the Southern and Eastern Alps. Permian magmatic rocks in the Southern Alps have been associated with a post-Variscan transtensional setting (e.g. Schaltegger and Brack 2007). In contrast, the geodynamic and tectonomagmatic setting of Middle Triassic magmatism is a matter of discussion yet. Predominant models invoke either magmatic arcs (e.g. Garzanti 1985, 1986; Castellarin et al. 1980, 1988) or transtensional-extensional rift dynamics (e.g. Crisci et al. 1984). Furthermore, the contribution of mantle and/or crustal components to the end-member melts, which erupted and intruded during the Middle Triassic magmatic episode in the Southern and Eastern Alps, is still uncertain.

Editorial handling: E. Gnos.

Electronic supplementary material The online version of this article (doi:10.1007/s00015-016-0234-3) contains supplementary material, which is available to authorized users.

✉ Alejandro Beltrán-Triviño
alejandro.beltran@erdw.ethz.ch

[1] Eidgenossische Technische Hochschule Zurich, Zurich, Switzerland

We analysed sandstones from Permian and Triassic sedimentary formations in the Southern and Eastern Alps (Fig. 1), in order to discriminate between a crustal and a mantle origin of the source rocks that supplied Permian and Triassic basins in the South-Alpine and Austroalpine palaeogeographic domains, and to evaluate the tectono-magmatic model of the Middle Triassic magmatism in this palaeogeographic context. This study presents new U–Pb dates and Hf isotopic compositions of detrital zircons, complemented by chemical analysis of detrital feldspar, garnet and chromian spinel.

Our results suggest mixed crust-mantle magma sources for the Permian magmatism, as similarly reported for Permian magmatic rocks in the Southern Alps (Schaltegger and Brack 2007). Furthermore, Hf isotopic compositions of the Middle Triassic volcaniclastic rocks indicate lesser contamination with crustal components than observed in the Permian volcaniclastic rocks, and the occurrence of chromian spinel and Mg-rich garnet in the heavy mineral suites of Carnian sandstones indicates a provenance partially affiliated to a mafic–ultramafic domain, possibly including a mid-ocean ridge (MOR) setting. These oceanic rocks presumably were related to a rift-drift process associated to an early stage of the Pangaea continental break-up. This scenario might has been controlled by hyperextension of the continental crust on back-arc type basins, possibly due to roll-back of the northward subduction of the Palaeotethys, within the geodynamic framework of the Middle Triassic proposed by Stampfli and Kozur (2006). We highlight the relevance of the Middle Triassic magmatic episode in the South-Alpine and Austroalpine domains, since this magmatic event marks the transition from the post-Variscan regime to the onset of the Alpine orogenic cycle.

2 Geological setting

2.1 South-Alpine and Austroalpine terranes from the post-Variscan to the Alpine cycle

Palaeogeographic reconstructions of the western Tethys (e.g. Stampfli and Borel 2002; Stampfli et al. 2002, 2013; Stampfli and Kozur 2006; Schettino and Turco 2009, 2011; von Raumer et al. 2003, 2013) suggest that the Austroalpine and South-Alpine terranes are part of the Adria-Apulia lithosphere (Fig. 2), which in turn was part of the NE margin of Gondwana supercontinent during the Early Palaeozoic.

In the Early Permian, the Variscan orogen collapsed, presumably due to rollback of the Palaeotethys subducting slab. Subsequently, Early Permian rift-like basin formation took place along with associated magmatism, and some of these basins in the Mediterranean region were oceanised due to extreme extension of the lithosphere (Stampfli and Kozur 2006). In Europe, according to McCann et al. (2006), the Early Permian was a period of crustal instability and re-equilibration, when transtensional activity led to the formation of a large number of basins, while the post-Variscan magmatism led to the extrusion of important volcanic successions. The late- and post-Variscan magmatic episodes were composed by many types of magmatism from calc-

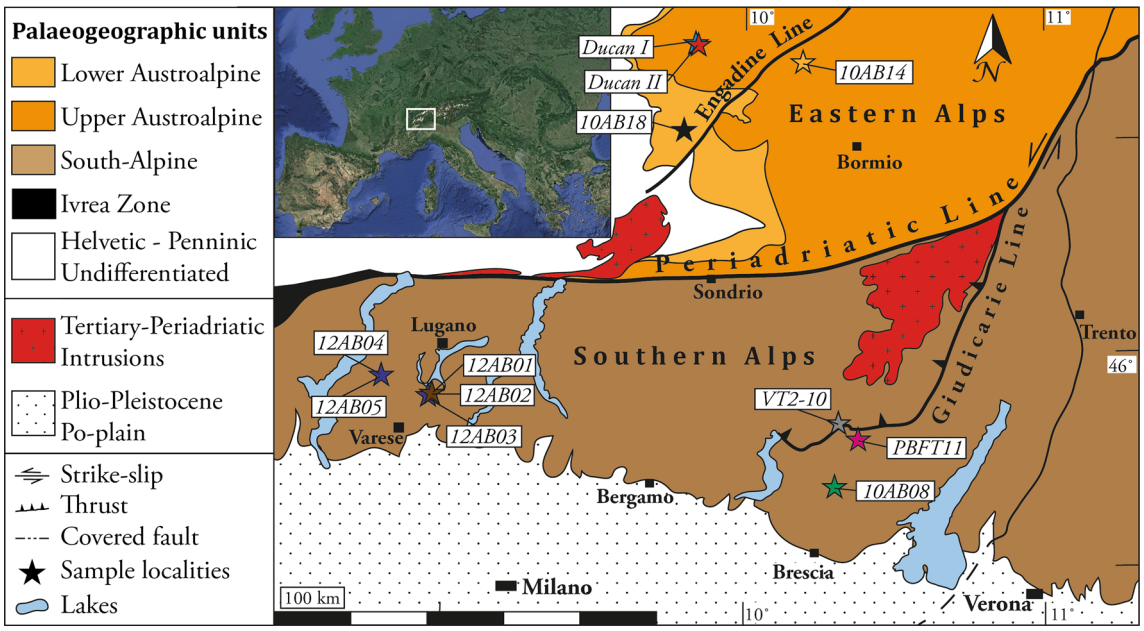

Fig. 1 Simplified map of the major palaeogeographic units of the western Southern Alps and the western Eastern Alps. Locations and codes of the investigated samples are shown. Modified from Schmid et al. (2004) and Schaltegger and Brack (2007)

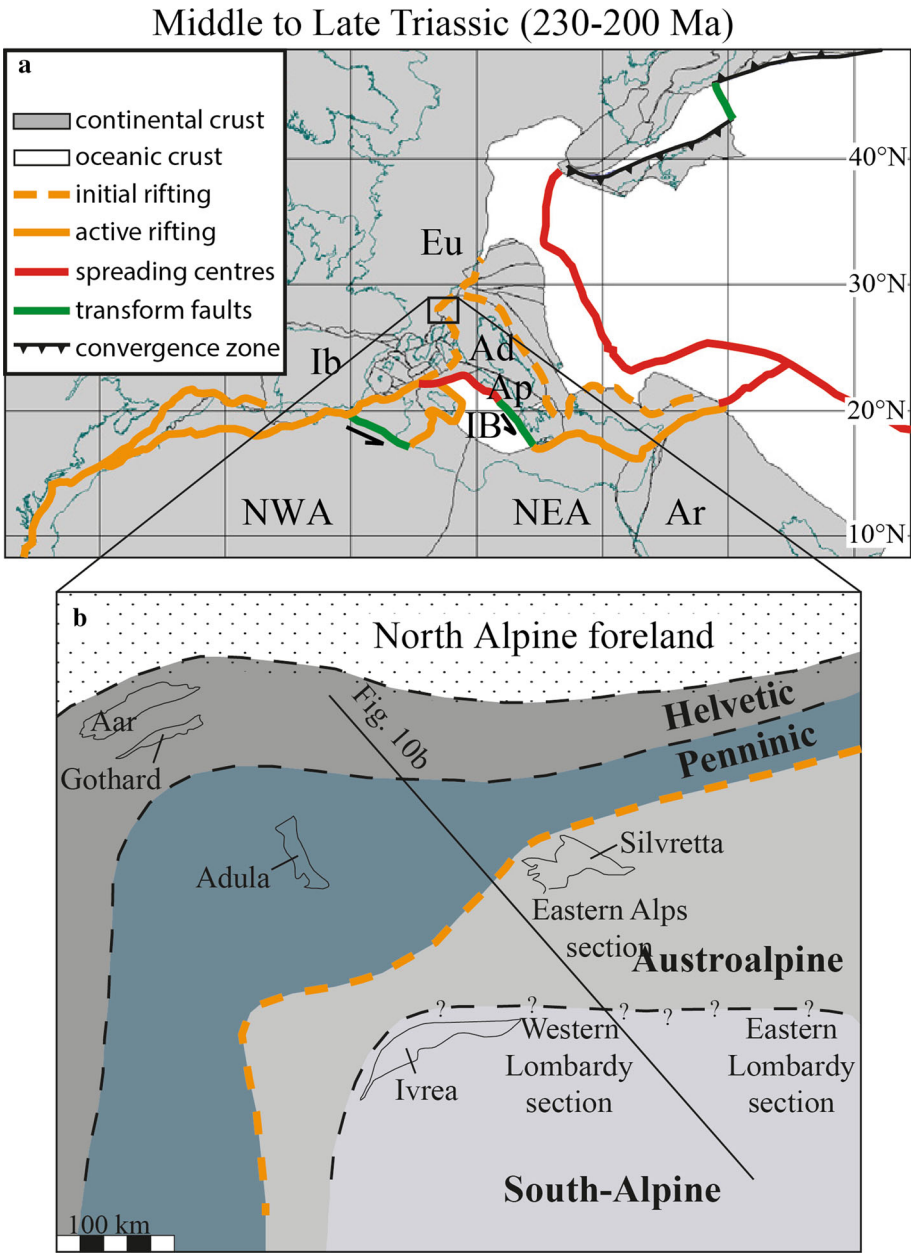

Fig. 2 Middle Triassic palaeogeography of the Alpine region: **a** Definition of the location of the Adria-Apulia continental lithosphere. The *grey* area represents continental lithosphere and *white* oceanic lithosphere. *Continuous orange lines*: active rifting; *dashed orange*: initial rifting; *red*: spreading centres; *green*: transform faults. Ad: Adria; Ap: Apulia; Ar: Arabia; Eu: Eurasia; Ib: Iberia; NEA: Northeastern Africa; NWA: Northwestern Africa; IB: Ionian basin (which is related to the Neotethys oceanic domain). Modified from Schettino and Turco (2011), and **b** Definition of the four main palaeogeographic domains in the Alps: Helvetic and Penninic (Eurasia continental lithosphere at the northern margin of the Alpine Tethys Ocean), Austroalpine and South-Alpine domains (Adria-Apulia continental crust at the southern margin of the AlpineTethys Ocean). Dashed orange line represents the initial rifting of the South Penninic – Ligurian Ocean. *Dashed black lines* represent boundaries between palaeogeographic domains. Names of present day basement units are given for geographical reference. Modified from Pfiffner (2009)

alkaline (i.e. re-melting arc and orogenic crust, e.g. Rottura et al. 1998) to anorogenic ring-dike complexes in Corsica-Sardinia (e.g. Traversa et al. 2003). These events are tentatively associated with the Late Palaeozoic-Early Mesozoic break-up of Pangaea.

In the Alpine terranes, the control of the post-Variscan tectonics has been attributed to Early Permian large-scale dextral strike-slip movements, which led to intracontinental basin formation and associated magmatism. Those events are recorded, for instance, in the South-Alpine Early Permian Collio Basin in the Southern Alps (e.g. Cassinis et al. 2007), in the Austroalpine Ruina Basin in the Eastern Alps (Dössegger 1974; Furrer 1985), and in the Helvetic Glarus Verrucano Basin (Letsch et al. 2015).

Late Permian-Middle Triassic strata in the Southern Alps document a long-term marine transgression, from the east to the westernmost part of the basin (Stampfli and Borel 2002). The Middle Triassic palaeogeography of this region was controlled by transtensive–transpressive tectonics, which resulted in differential uplift and subsidence of blocks (e.g. Stockar et al. 2012). The Middle Triassic magmatism is widely recognised in basins along the Southern (e.g. Mundil et al. 1996) and Eastern Alps (Furrer et al. 2008).

The timing of the onset of the Alpine orogenic cycle is still a matter of debate. According to Bertotti et al. (1993), the Norian activation of extensional faults in the Southern Alps represents the onset of the Alpine extension, and

consequently, the Middle Triassic tectonomagmatic activity would not be related to the rifting of the Alpine Tethys and the onset of the Alpine orogenic cycle. In contrast, other investigations suggest that the onset of the Alpine cycle could be placed in the Carnian, a period corresponding with the closure of the eastern Palaeotethys and the initial rifing in the Central Atlantic-Alpine domain (Stampfli and Kozur 2006 and references therein).

During the Late Triassic–Jurassic, rifting and drifting processes led to the opening of the Alpine Tethys oceanic domain, which separated the Eurasia and Adria-Apulia continental blocks. Eurasia is represented by the Helvetic and the Penninic domains while the Southalpine and Austroalpine domains represent marginal regions of the Adriatic-Apulia continental lithosphere (Fig. 2b). The so-called South Penninic or Ligurian Ocean, the first oceanic lithosphere of the Alpine Tethys oceanic system, progressively opened from the West (e.g. Schettino and Turco 2011). During this time, passive continental margins developed on both sides of the ocean.

2.2 Middle Triassic magmatism: geology and geochemistry

The widespread Middle Triassic volcanic products, which mainly consist of pyroclastic flows and lavas, are interbedded with shallow marine sequences, continental and transitional deposits of Anisian-Ladinian-Carnian age in the Southern and Eastern Alps (e.g. Mundil et al. 1996; Furrer et al. 2008). In the Southern Alps, the geochemistry of magmatic products shows calc-alkaline signatures similar to those of convergent margins (e.g. Castellarin et al. 1980, 1988; Crisci et al. 1984; Garzanti 1985; Bertotti et al. 1993; Cassinis et al. 2008). However, in the Alpine area it is widely accepted that the Permian transcurrent (Schaltegger and Brack 2007) and the Late Triassic transtensional movements (Bertotti et al. 1993) dominated the tectonic framework of this region.

The apparent disagreement between the tectonic environment and the type of erupted magmas is tentatively explained by partial melting of an upper mantle, during early stages of rifting, that has been deeply modified by the previous Variscan orogeny and contamination by crustal material (Crisci et al. 1984). Other works recognised the relevance of the geochemical inheritance in lithospheric processes, where the calc-alkaline character of Triassic volcanics is an inherited signature of the previous Variscan subduction, as documented in eastern Mediterranean Triassic basins (Dixon and Robertson 1993; Robertson 2006). In contrast, other investigations associated the Middle Triassic magmatism with the syn-depositional development of a Pacific-type volcanic arc in the western Southern Alps (Garzanti 1985), and moreover, Castellarin et al. (1988) suggested that the calc-alcakaline to shoshonitic chemistry of the Middle Triassic magmatic rocks indicate an orogenic event within a compressional setting, due to the subduction of a visco-plastic continental lithospheric body under the Southern Alps.

Fig. 3 Composite Permian–Triassic lithostratigraphic section of the western Southern Alps and Permian–Jurassic of the western Eastern Alps with the known framework of radiometric ages of Permian magmatic and Middle Triassic volcaniclastic rocks (references inside). *Red stars* indicate the stratigraphic position of the investigated samples. Compiled from Furrer (1985), Furrer et al. (2008), Cassinis et al. (2007, 2008), Schaltegger and Brack (2007), Stockar et al. (2012) and Gretter et al. (2013). Time scale from Cohen et al. (2013; updated) ▶

3 Samples and methods

3.1 Samples

Volcaniclastic sandstones and tuff layers were sampled in sections with bio- and chronostratigraphic control that allows correlation along with the Permian–Triassic record in the region. The location of the analysed samples is illustrated in Fig. 1. Their stratigraphic position, grouped in three composite sections, is shown in Fig. 3. From the Austroalpine domain in the Eastern Alps of eastern Switzerland, we analysed zircons from two ash layers interbedded in intraplatform basinal limestones of the Middle Triassic Prosanto and Altein formations (samples named Ducan I and Ducan II, respectively, in Furrer et al. 2008) and compared those with detrital zircons from the Middle Triassic shallow marine calcareous sandstones of the Fuorn and the Middle Jurassic Saluver formations. The latter two are described in detail in Beltrán-Triviño et al. (2013).

We investigated two localities of the Southern Alps in northern Italy and southern Switzerland: the region of Bagolino-Val Sabbia (eastern Lombardy) south of the Giudicarie lineament, and the region between Monte San Giorgio and Mesenzana (western Lombardy) to the south-southwest of the city of Lugano. From the eastern Lombardy section (Fig. 3) we analysed: (1) Early Permian volcaniclastics (Dasdana beds VT2-10), which are presumably related to extrusive episodes of a sublacustrine silicic cryptodome (Breitkreuz et al. 2002), (2) a volcaniclastic horizon (Pietra Verde) in Middle Triassic pelagic sediments of the upper Buchenstein Fm (PBFT11); and (3) the early Late Triassic Val Sabbia Sst. (10AB08), which consists of volcaniclastic litharenites described in Beltrán-Triviño et al. (2013).

The analysed samples in the western Lombardy region (Fig. 3) are from volcaniclastic horizons in the Anisian fluvio-deltaic deposits of the Bellano Fm (12AB03,

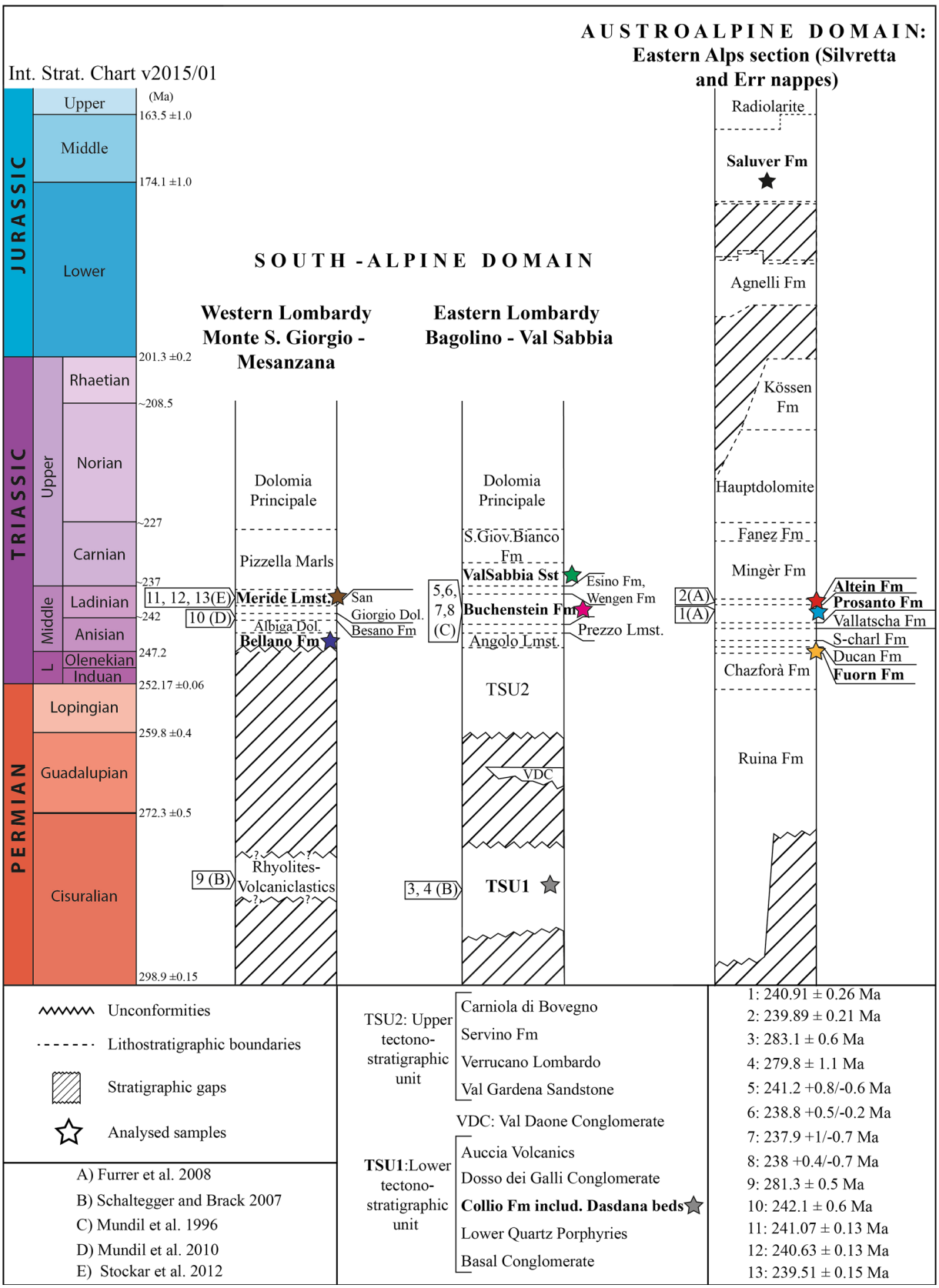
AUSTROALPINE DOMAIN:
Eastern Alps section (Silvretta and Err nappes)
Int. Strat. Chart v2015/01
SOUTH-ALPINE DOMAIN
Western Lombardy
Monte S. Giorgio - Mesanzana
Eastern Lombardy
Bagolino - Val Sabbia
(Ma)
JURASSIC
Upper
Middle
Lower
163.5 ±1.0
174.1 ±1.0
TRIASSIC
Upper
Middle
L
Rhaetian
Norian
Carnian
Ladinian
Anisian
Olenekian
Induan
201.3 ±0.2
~208.5
~227
~237
~242
247.2
252.17 ±0.06
PERMIAN
Lopingian
Guadalupian
Cisuralian
259.8 ±0.4
272.3 ±0.5
298.9 ±0.15
Radiolarite
Saluver Fm
Agnelli Fm
Kössen Fm
Hauptdolomite
Fanez Fm
Mingèr Fm
Chazforà Fm
Ruina Fm
Dolomia Principale
Pizzella Marls
Meride Lmst.
Albiga Dol.
Bellano Fm
San Giorgio Dol.
Besano Fm
Rhyolites-Volcaniclastics
S.Giov.Bianco Fm
ValSabbia Sst
Buchenstein Fm
Angolo Lmst.
Esino Fm,
Wengen Fm
Prezzo Lmst.
TSU2
VDC
TSU1
Altein Fm
Prosanto Fm
Vallatscha Fm
S-charl Fm
Ducan Fm
Fuorn Fm
11, 12, 13(E)
10 (D)
9 (B)
5,6, 7,8 (C)
3, 4 (B)
2(A)
1(A)
Unconformities
Lithostratigraphic boundaries
Stratigraphic gaps
Analysed samples
A) Furrer et al. 2008
B) Schaltegger and Brack 2007
C) Mundil et al. 1996
D) Mundil et al. 2010
E) Stockar et al. 2012
TSU2: Upper tectono-stratigraphic unit
Carniola di Bovegno
Servino Fm
Verrucano Lombardo
Val Gardena Sandstone
VDC: Val Daone Conglomerate
TSU1: Lower tectono-stratigraphic unit
Auccia Volcanics
Dosso dei Galli Conglomerate
Collio Fm includ. Dasdana beds
Lower Quartz Porphyries
Basal Conglomerate
1: 240.91 ± 0.26 Ma
2: 239.89 ± 0.21 Ma
3: 283.1 ± 0.6 Ma
4: 279.8 ± 1.1 Ma
5: 241.2 +0.8/-0.6 Ma
6: 238.8 +0.5/-0.2 Ma
7: 237.9 +1/-0.7 Ma
8: 238 +0.4/-0.7 Ma
9: 281.3 ± 0.5 Ma
10: 242.1 ± 0.6 Ma
11: 241.07 ± 0.13 Ma
12: 240.63 ± 0.13 Ma
13: 239.51 ± 0.15 Ma

12AB04, 12AB05), and in the Ladinian carbonates of the Meride Lmst. (12AB01, 12AB02).

3.2 Methods

High voltage pulse power technology (Selfrag system, SELFRAG AG, Switzerland) was used for sample fragmentation. Heavy mineral and detrital zircon separation followed the standard procedures (e.g. Mange and Maurer 1992) at ETH Zurich facilities. Bromoform (2.89 g/cm^3) and Methylene iodide ($\delta = 3.32$ g/cm^3) were used for density separation out of the sieve fraction 400-63 µm. Hand picking of zircon grains from the heavy mineral concentrates was randomly performed in each sample. After mounting in the epoxy-pill, grains were polished. Cathodoluminescence (CL) imaging was carried out on the zircons to evaluate the magmatic zonation, metamorphic origin and rims, or inherited cores. For this purpose, we used the Vega 3 W-SEM at ScopeM/Swiss Federal Institute of Technology ETHZ and a Vega CamScan at University of Lausanne. Rims were preferentially analysed in order to date the last growth stage of each grain, but also inherited cores were analysed when the size of the core was large enough for measurement (>30 µm).

U–Pb geochronology of detrital zircons was performed through laser ablation inductively coupled mass spectrometry (LA-ICP-MS), the Lu–Hf concentrations were measured on a multiple collector inductively coupled plasma mass spectrometer (MC-ICP-MS).

Single-mineral geochemical compositions of feldspars, garnets and chromian spinel were measured on an electron microprobe instrument at ETH Zurich facilities. The analytical parameters and specifications of the methods and procedures are described in the Online Resource 1.

4 Results and discussion

Including in this chapter our previous U–Pb and Hf data (Beltrán-Triviño et al. 2013), we present in the following lines our main results from detrital zircon, garnet, chromian spinel and feldspar. The obtained detrital zircon U–Pb geochronology and Lu–Hf databases for this work can be examined in the Online Resources 2, and 3.

4.1 Eastern Alps section (Austroalpine domain)

4.1.1 Fuorn Formation, early Anisian (10AB14)

Zircon grains from the Fuorn Fm are mainly prismatic fragments and euhedral crystals. Only a few sub-rounded

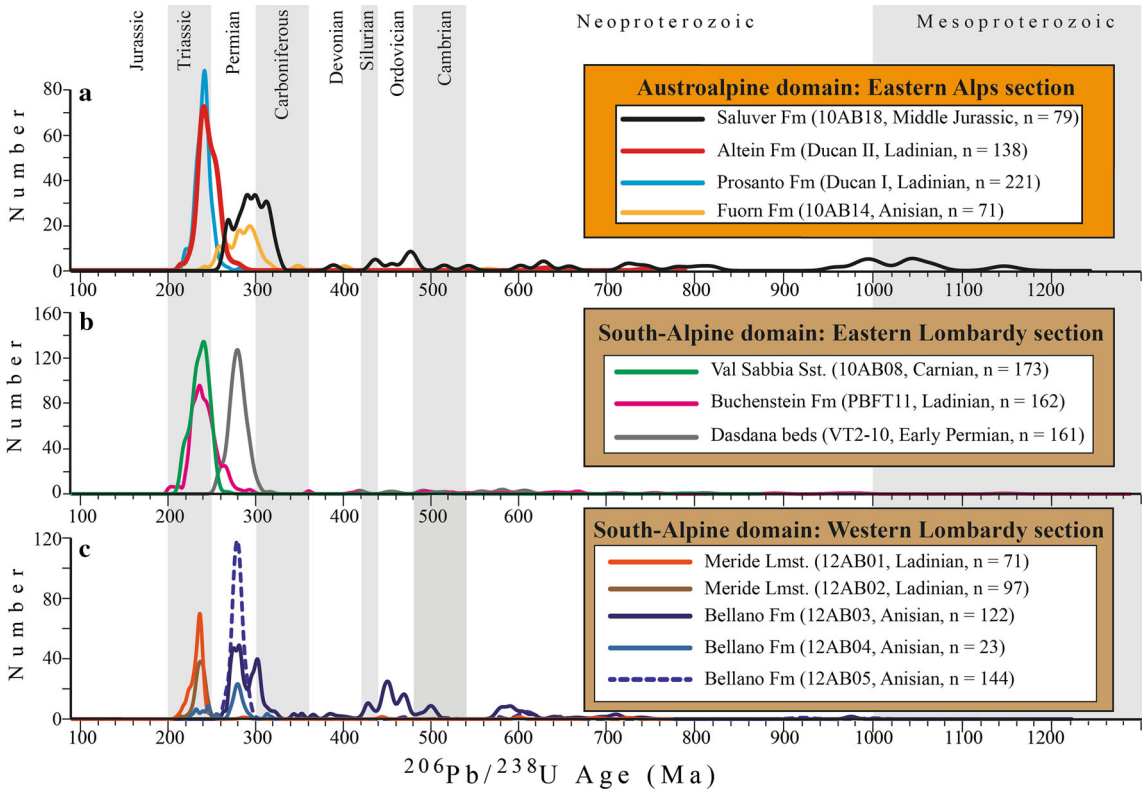

Fig. 4 Probability density distribution of concordant detrital zircon ages (Ma). Concordia diagrams are not shown. Numbers in brackets next to the sample labels represent the number of analyses. **a** Eastern Alpine formations. Fuorn and Saluver formations taken from Beltrán-Triviño et al. (2013), **b** Southern Alps units, eastern Lombardy section; and **C** Southern Alps units, western Lombardy section

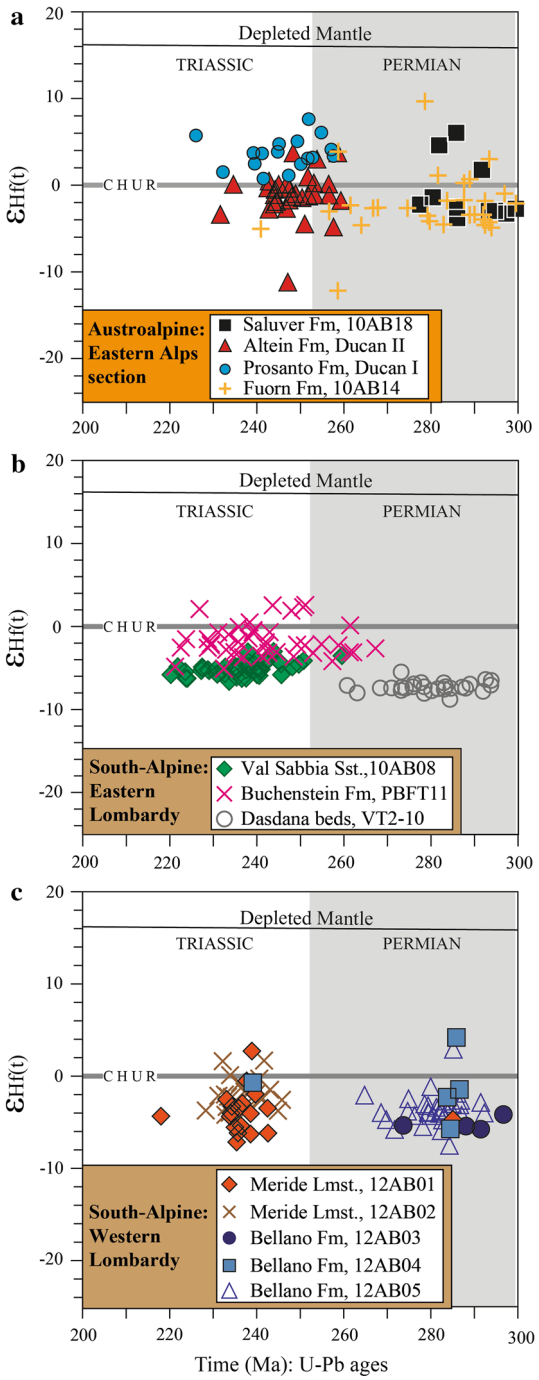

Fig. 5 Hf-isotope systematics of Permian and Triassic detrital zircons, showing εHf(t) versus $^{206}Pb/^{238}U$ crystallization ages in Ma: **a** Eastern Alpine formations. Fuorn and Saluver formations taken from Beltrán-Triviño et al. (2013); **b** Southern Alps units, eastern Lombardy section; and **c** Southern Alps units, western Lombardy section

grains were found. Most of the zircons show well-developed oscillatory zoning and frequently, inherited cores (Online Resource 4a). Late Carboniferous and Early Permian populations dominate the detrital zircon age spectrum (Fig. 4a), with peaks at ca. 290 and 280 Ma. A minor Late Permian-Early Triassic population with a peak at ca. 260 Ma is also determined. Inherited cores yielded Neoproterozoic-Cambrian (ca. 560–530 Ma), Devonian (ca. 400 Ma) and Early Carboniferous (ca. 345 Ma) ages.

Nearly all εHf(t) values of Carboniferous-Permian zircons plot between −5 and +4 (Fig. 5a) indicating partial contribution from crustal components to the melts. The Fuorn Fm mainly was supplied from Permian post-Variscan volcano-sedimentary (e.g. Verrucano-type), and volcanic and plutonic rocks, which explains the abundance of euhedral zircons. The age of the components of the magmatic sources (TDM_2) are between ca. 2.3 and 0.7 Ga (Fig. 6a); however, the points cluster around 1.3 Ga (range from 1.65 to 1.45 Ga).

4.1.2 Prosanto Formation, late Anisian–early Ladinian (Ducan I)

We analysed part of the same sample of an ash layer previously dated by isotope dilution thermal ionization spectrometry (ID-TIMS) at 240.91 ± 1.4 Ma (Furrer et al. 2008). The sample holds zircon grains with euhedral to sub-euhedral morphologies. Abundant inherited cores, magmatic growth zones and typical oscillatory zoning are identified in CL images (Online Resource 4b). Magmatic growth rims often are very narrow and, hence, in order to avoid age mixing, we mainly measured isotopic concentrations in the cores or broader rims. A total of 221 analyses in rims and inherited cores define the age distribution shown in Fig. 4a. In prismatic zircons, 113 analyses in rims define a weighted mean $^{206}Pb/^{238}U$ age of 244.2 ± 1.4 Ma (MSWD = 6.3). 108 analysed cores yielded Late Carboniferous (ca. 298 Ma), Late Permian (ca. 263 Ma) and Triassic (ca. 250–240 Ma) ages. The latter is the most abundant inherited-core age population, with a cluster around ca. 245 Ma.

Late Permian inherited cores and Triassic zircons yielded only positive εHf(t) values (Fig. 5a) ranging from +0.7 to +7.6. These values indicate very little contribution of crustal components and more juvenile character of the magma sources, including the sources of the inherited cores. The crustal residence time given by the TDM_2 model ages (Fig. 6a) ranges from ca. 1.31 to 0.88 Ga.

4.1.3 Altein Formation, middle Ladinian (Ducan II)

This sample of ash layer was previously dated by ID-TIMS at 239.89 ± 0.21 Ma (Furrer et al. 2008). The zircon fragments are prismatic and euhedral crystals are very common with well-developed oscillatory zoning (Online Resource 4c). Abundant inherited cores are present and the peripheral magmatic rims are rather narrowly zoned, as described for the pyroclastic horizon in the Prosanto Fm (see above). A total of 138 analyses in rims and inherited

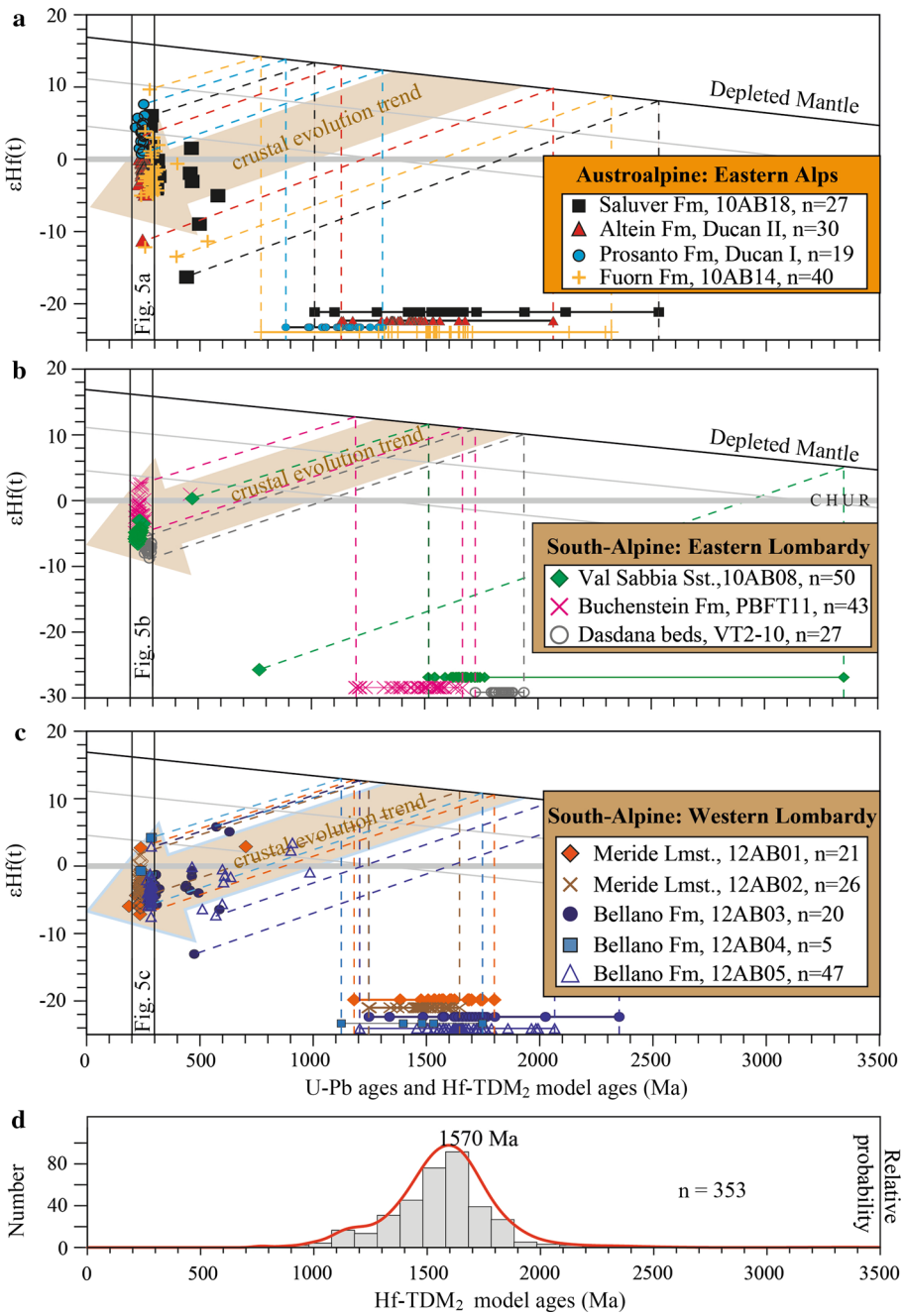

Fig. 6 Hf-isotope systematics of detrital zircons, showing εHf(t) versus time in Ga: **a** Eastern Alpine Fuorn and Saluver formations taken from Beltrán-Triviño et al. (2013); **b** Southern Alps units, eastern Lombardy section; and **c** Southern Alps units, western Lombardy section. **a-c** The time axis represents the values of $^{206}Pb/^{238}U$ crystallisation age of single zircons, and the second the two-stage Hf depleted mantle model ages (Hf-TDM2) estimated for single zircons. *Coloured horizontal lines* with symbols indicate the time range (Ga) of Hf-TDM2 of each sample. *Leaned coloured dashed lines* show the evolution of εHf for representative zircons from their crystallization age back to the depleted mantle growth curve. *Vertical coloured lines* indicate the value of the Hf-TDM2 in Ga for representative zircons. **d** Histogram and probability density distribution of the Hf-TDM2 of the analysed detrital zircons

cores define the age distribution illustrated in Fig. 4a: 65 rims reveal a weighted mean $^{206}Pb/^{238}U$ age of 243.7 ± 1.3 Ma (MSWD = 2.6), 73 cores yielded a few Neoproterozoic (ca. 660, 570, 560 Ma) and abundant Permian ages spanning ca. 280–250 Ma.

Negative εHf(t) values (Fig. 5a) predominate, covering a range between ca. −5 to 0, with one outlier at ca. −11, and 3 points between +3 to +4. In general, these values contrast with the positive εHf(t) trend of the zircons from the ash layer in the early Ladinian Prosanto Fm. The TDM_2 model ages (Fig. 6a) span 1.67–1.12 Ga, which are older than those estimated for the ash layer of the Prosanto Fm. One outlier yielded the oldest TDM_2 at 2.05 Ga which correspond to the lowest εHf(t) of ca. −11.

4.1.4 Saluver formation, member B, Middle Jurassic, (10AB18)

The zircon grains of the Saluver Fm are sub-rounded to sub-euhedral, which contrasts with the euhedral morphologies reported above. Oscillatory zoning and growth bands are common (Online Resource 4d), as well as inherited cores.

Often, the zircons show a thin metamorphic rim. The detrital zircons reveal a composite age spectrum (Fig. 4a) dominated by Late Carboniferous-Early Permian zircons (ca. 320–270 Ma). Smaller Ordovician and Silurian populations are noted (post-Cadomian, ca. 465 and 430 Ma), and few Proterozoic (Cadomian and older) zircons of ca. 1010, 960, 710, 610 Ma. According to the sub-rounded morphology, some of the Proterozoic and also Early Palaeozoic zircons might be considered as reworked from older basement cover sediments. Inherited cores may indicate re-melting of Ordovician–Silurian and older crustal components or magmatic overgrowth during the late stages of the Variscan orogenic cycle.

In the Carboniferous and Permian zircons of the Saluver Fm, εHf(t) values range between −3 and +7 (Fig. 5a), comparable with those of the Fuorn Fm. This indicates moderately juvenile to moderately crustal-contaminated magma sources. In contrast, sparse Neoproterozoic to Early Palaeozoic Saluver zircons (Fig. 6a) show a widespread distribution in the negative field of εHf (t) between −16 to +2. The values of TDM_2 model age (Fig. 6a) range between ca. 2.5 and 1.0 Ga and they group between 1.65 and 1.45 Ga, partially overlapping the TDM_2 model ages of Fuorn and Altein formations.

4.1.5 Summary of the Eastern Alps section

Fuorn and Saluver formations were mainly supplied from post-Variscan (Late Carboniferous-Permian peaks in Fig. 4a) reworked sources. Early Palaeozoic and Proterozoic ages presumably represent reworked zircons from sedimentary sources and the inherited cores evidence the re-melting of Variscan and older crust components during the post-Variscan magmatism.

Our analysis of the ash layers in the Prosanto and Altein formations (Ducan I: 244.2 ± 1.4 Ma, and Ducan II: 243.7 ± 1.3 Ma, Fig. 4a) suggests that the age is the same within the errors. The same horizons have been precisely dated by ID-TIMS at 240.91 ± 0.26 and 239.89 ± 0.21 Ma, respectively (Furrer et al. 2008). However, our dataset indicate a high age dispersion possibly due to source mixing and/or analytical scatter, and furthermore, Pb loss of the U–Pb system. The high MSWD of 6.3 for Ducan I indicates that there is a geological age dispersion, which does not allow us to make a mean age. The MSWD of 2.6 for Ducan II indicates less dispersion, but still too high to calculate a mean age. The late Anisian–Ladinian magmatic episodes documented by the studied ash layers are not recorded in the Middle Jurassic Saluver Fm. Evidently, Middle Triassic sources were not available for the Saluver basin in the Austroalpine domain.

Most of the εHf(t) analyses of the studied Permian and Triassic zircons in Austroalpine Triassic—Jurassic units yielded negative values, indicating contribution of crustal material into the magma sources, with the exception of the ash layer Ducan I (Prosanto Fm, Fig. 5a) that only indicated positive values, evidencing rather juvenile magma sources. Comparing with the Ducan II pyroclastic horizon (Altein Fm, Fig. 5a), two possible scenarios can explain this apparent contrast: (1) heterogeneous magma reservoirs emplaced at different crustal levels, and almost-coevally erupted in a transtensional tectonic setting. One pulse produced from a reservoir with predominant mantle components (Ducan I in Prosanto Fm) and a second pulse from a reservoir with higher influence of crustal components (Ducan II in Altein Fm). (2) The second scenario assumes the existence of a magmatic system that admitted a first eruptive event (Ducan I) when the magma sources were dominated by mantle components, and a second pulse (Ducan II) produced when the magma sources were influenced by crustal components, indicating a rapid evolution of the root of the magmatic system.

The TDM_2 model ages point that the hybrid age of the components of the magma sources of the ash layer in the Prosanto Fm (Ducan I, Fig. 6a) range between ca. 1.31 and 0.88 Ga, while the magma sources of the upper pyroclastic horizon in the Altein Fm (Ducan II, Fig. 6a), which also exhibit higher proportion of crustal influence, show a range between 1.67 and 1.12 Ga. These differences in model ages and εHf(t) are due to mixing of different source compositions.

4.2 Southern Alps, eastern Lombardy section (South-Alpine domain)

4.2.1 Dasdana beds, Early Permian (VT2)

Zircon crystals are euhedral to sub-euhedral and exhibit well-developed internal structures as inherited cores, oscillatory zoning and growth bands (Online Resource 4e). The zircon age spectrum is shown in Fig. 4b, which is dominated by Early Permian (post-Variscan) ages spanning ca. 315–260 Ma with a weighted mean at ca. 280 Ma. Inherited cores yielded Paleoproterozoic (ca. 1960 Ma), Neoproterozoic (ca. 790, 740, 650, 590, 570, 550 Ma), Middle and Late Cambrian (ca. 515, 500–480 Ma), Late Ordovician-Early Silurian (ca. 450–440 Ma), early Devonian (ca. 414 Ma) and Late Carboniferous—Early Permian (ca. 315-260 Ma) ages. The high abundance of inherited cores and the heterogeneity of the ages suggest the re-melting of components of the Variscan and post-Variscan crust.

Estimated εHf(t) of inherited cores and rims exhibit negative values (Fig. 5b), indicative for crustal influence on the magma sources. The εHf(t) values range from −8.8 to −5.5 with a mean value around −7.3. The TDM_2 model ages (Fig. 6b) show a rather narrow distribution between 1.94 and 1.72 Ga.

4.2.2 Buchenstein Formation, Anisian–Ladinian (PBFT11)

Most of the zircon crystals are elongated and exhibit euhedral morphologies. Oscillatory zoning is a common feature and abundant inherited cores are identified (Online Resource 4f). Middle Triassic ages dominate the age spectrum (Fig. 4b) with a peak at ca. 235 Ma in a composite range from ca. 260 to 220 Ma. Precambrian inherited cores yielded ages in a range from ca. 2750 to 553 Ma. Palaeozoic inherited cores were also determined: Permian–Triassic cores are the most abundant (ca. 285–240 Ma), but there are also Cambrian–Ordovician (ca. 530–460 Ma) and one Devonian (ca. 391 Ma) core.

Hf isotopic compositions (Fig. 5b) reveal a range of εHf(t) values from −5.1 to +2.6. However, negative values predominate, indicating a moderate influence of the crust on the magma sources. The TDM_2 model ages (Fig. 6b) span from 1.67 to 1.19 Ga.

4.2.3 Val Sabbia Sandstone, Carnian (10AB08)

Zircons delivered by this fluvio-deltaic sandstone are sub-rounded to sub-euhedral with defined internal structures such as oscillatory zoning and abundant inherited cores (Online Resource 4 g). Middle Triassic (Ladinian) zircons dominate the age spectrum (ca. 239 Ma; Fig. 4b). One inherited core yielded a Neproterozoic age (ca. 770 Ma) and one core dated at ca. 500 Ma (Cambrian). Most of the inherited cores have Late Permian-Early Triassic ages (ca. 260–240 Ma).

The range of εHf(t) is defined between ca. −6.6 and −3 (Fig. 5b) providing evidence for the contribution of the crust to the parental magmas. Two outliers yielded εHf(t) values of +0.3 and −25.7, and correspond to inherited cores dated at ca. 500 and 770 Ma, respectively. The TDM_2 ages (Fig. 6b) cluster between 1.76 and 1.51 Ga. One outlier at ca. 3.35 Ga corresponds to the ca. 700 Ma inherited core.

4.2.4 Summary of the eastern Lombardy section

We observe a deviation of the U–Pb age distributions with respect to the depositional ages of the Middle Triassic Buchenstein and the early Late Triassic Val Sabbia Sst. (Figs. 3, 4b). The peak of the main age population in the Buchenstein Fm (235.3 ± 1.9 Ma) deviates ca. 1.5% from a previous accurate ID-TIMS dating at 239.3 ± 0.2 Ma (Mundil et al. 1996; Brack et al. 2007), and is slightly younger than the depositional age (Ladinian). However, this can be interpreted as identical considering the uncertainty of 2% inherent to laser ablation U–Pb dating (Schaltegger et al. 2015).

In contrast, zircon U–Pb ages from the Carnian Val Sabbia Sst. locate the peak of the main population at ca. 239 Ma (Ladinian). This indicates an older age than expected, since it has been suggested that the Val Sabbia Sst. was a syn-magmatic deposit, derived from a Carnian magmatic arc (Garzanti 1985). The presence of crystals with ages older than Carnian have two possible causes: (1) the presumable existence of older sediment sources (e.g. Late Permian–Early Triassic igneous rocks), or (2) the abundant presence of older xenocrysts and xenoliths within the melts.

All analysed Permian and Triassic zircons in sandstones and pyroclastic horizons from the eastern Lombardy section yield εHf(t) values between −9 and +2 (Fig. 5b). According to the mean εHf(t) value of each unit, it is possible to discriminate three different types of the magma sources. The highest proportion of crustal influence on magma reservoirs has been determined for the Permian Dasdana zircons (mean εHf(t) = −7.3), which also hold the oldest TDM_2 model age range (1.94–1.72 Ga) shown in Fig. 6b. Magma sources with lower portion of the crust influence are found in the early Late Triassic Val Sabbia Sst., which has a mean of εHf(t) = −5.1 (Fig. 5b) and TDM_2 model age range from 1.76 and 1.51 Ga (Fig. 6b). Middle Triassic Buchenstein zircons show the lowest portion of crustal contribution to the magma sources (εHf(t) = ca. −1.6; Fig. 5b), also yielding the youngest TDM_2 model age range of 1.67–1.19 Ga (Fig. 6b).

4.3 Southern Alps, western Lombardy section (South-Alpine domain)

4.3.1 Bellano Formation (early Anisian)

Three samples were taken from different stratigraphic levels in the area between Monte San Giorgio (southern Switzerland) and the village of Mesenzana (northwestern Italy). In the Mesenzana area, the lower sample (sandstone 12AB05) delivered sub-euhedral to sub-rounded zircon grains (Online Resource 4 h). Permian U–Pb ages predominate (Fig. 4c) with a peak at ca. 280 Ma (post-Variscan) corresponding only to magmatic rims. Particularly, ca. 52% of the measurements were performed on inherited cores because the peripheral magmatic growth zones were narrow. However, the age distribution of cores and rims overlaps the main peak. Older inherited cores were dated at ca. 1000, 900, 650–600, 500, 460 Ma, and the main population ranges ca. 320–270 Ma.

On top of the latter sandstone, bentonites interpreted as a pyroclastic horizon in the Bellano Fm (12AB04) delivered angular fragmented zircon prisms with oscillatory zoning of magmatic origin (Fig. 4i). Inherited cores are abundant, and only on 5 grains it was possible to date peripheral magmatic

rims (total n = 23; Fig. 4c). The main population consists of inherited cores that yielded an age cluster at ca. 280 Ma (post-Variscan). The analysed rims yielded a weighted mean of 240.2 ± 8.9 Ma (MSWD = 10). The significance of this age peak is constrained by the high value of the MSWD, and we interpreted that another geological scatter is present in the data, e.g. radiogenic perturbations during post-depositional processes. However, the value approximately correlates with the depositional age of the Bellano Fm and therefore, it might record the first magmatic episode of the early Middle Triassic in the region.

In the Monte San Giorgio area, zircons from a volcaniclastic layer (12AB03) exhibit contrasting morphologies between sub-rounded grains and elongated sub-euhedral prismatic fragments (Online Resource 4j). The results show three main populations (Fig. 4c): (1) Neoproterozoic inherited cores of 1550, 960, 700 and mainly 580 Ma. (2) Cambrian–Silurian cores ranging from ca. 500 to 430 Ma, and (3) main population of Late Carboniferous to Early Permian zircons, which also include inherited cores yielding the same age range. It peaks at ca. 280 Ma and overlaps with the other two samples analysed for the Bellano Fm (Fig. 4c). The spectrum of the Monte San Giorgio sample contrasts with those obtained for the sandstone 12AB05 and the ash layer 12AB04 in the Mesenzana area. The early Palaeozoic detrital population in the Bellano Fm of the Monte San Giorgio reveals an additional source of sediments, presumably a reworked Permian sedimentary cover of the pre-Alpine basement, which evidently, was not available for the Bellano basin in the Mesenzana area.

Permian zircons and inherited cores of the Bellano Fm yield εHf(t) values that cluster below the CHUR in a range from ca. −8 to −1 (Fig. 5c), indicating that the crustal contribution on the magma sources predominates. The range of εHf(t) values matches the Permian zircons and inherited cores of the Austroalpine Fuorn and Saluver formations (Fig. 5a) and in the Southalpine Dasdana beds (Fig. 5b).

TDM_2 model ages of the Bellano Fm samples are shown in Fig. 6c. The sandstone 12AB05 span ca. 2.06–1.2 Ga with a cluster from ca. 1.78 to 1.45 Ga. Inherited cores of Neoproterozoic—early Palaeozoic crystallization ages yield the older Hf TDM_2 model ages. The ash layer 12AB04 exhibits TDM_2 ages in a range from ca. 1.74 to 1.12 Ga. The sandstone 12AB03 yield TDM_2 ages between 2.34 and 1.24 Ga, though the points grouped in a range from ca. 1.8 to 1.57 Ga. The analysed Permian zircons from the three samples of the Bellano Fm revealed TDM_2 model ages in a common range from ca. 1.75 to 1.45 Ga.

4.3.2 Meride Limestone (Ladinian)

Two samples of the Meride Lmst. were taken from the Monte San Giorgio area in southern Switzerland. The lower sample derived from calcareous sandstones (12AB02) and the upper one is from a pyroclastic horizon (12AB01) on top of the former. Sample 12AB02 delivered sub-euhedral zircon grains and sparse inherited cores have been identified (Online Resource 4 k). The main population includes Middle Triassic zircons with a peak at ca. 238 Ma (Fig. 4c). Inherited cores yielded Early Triassic ages (ca. 250–240 Ma). The ash layer (12AB01) provided sub-euhedral and euhedral fragmented prisms (Online Resource 4 l). The main population (Fig. 4c) yielded a weighted average of 236.34 ± 0.62 Ma, MSWD = 5.8.

The Triassic zircon εHf(t) values of the two samples of the Meride Lmst. show a range between ca. −7 to +2 (Fig. 5c) evoking crustal contribution to the magma sources. The samples exhibit also a common TDM_2 model age range from 1.65 to 1.45 Ga (Fig. 6c). However, the ash layer 12AB01 yielded older TDM_2 model ages (ca. 1.8–1.7 Ga) which correlate with the most negative εHf(t) values (ca. −7). The youngest TDM_2 model ages of both samples (ca. 1.4–1.2 Ga) concur with the positive εHf(t) values indicating less contribution of crustal components on the magma sources.

4.3.3 Summary of the western Lombardy section

The Bellano Fm in the Mesenzana area was primarily sourced in Permian igneous rocks, while in the area of Monte San Giorgio the Bellano Fm was supplied from Variscan and post-Cadomian basement, or from a sedimentary cover of Verrucano Lombardo type (Fig. 4c). This finding highlight the presence of basement elements older than Variscan within the Southalpine domain.

The detrital zircon U–Pb ages of an ash layer of the Anisian Bellano Fm (12AB04) in the Monte San Giorgio area shows a scattered distribution between 249 ± 2.0 and 239 ± 3.1 Ma (online resource 2), which includes the oldest Triassic ages (Olenekian-Ladinian) recorded in this work.

The zircon age distributions of a volcaniclastic (12AB02) and a pyroclastic horizon (12AB01) in the upper Meride Lmst. overlap at ca. 237 Ma (Fig. 4c) indicating a primary source in Ladinian volcanic rocks. Consequently, the intraplatform basin with restricted circulation (Furrer 1995) received episodic volcanic input. The age peak correlates with high precision ages obtained in the upper Meride Lmst. at Monte San Giorgio (239.51 ± 0.15 Ma, Stockar et al. 2012; Fig. 3).

The Permian magmatic rocks that supplied with detritus the Bellano basin during the Middle Triassic shared a signature of crustal influence on the magma sources, as shown by consistent negative εHf(t) values in Fig. 5c. The Meride Lmst. represents a Ladinian syn-magmatic sequence, which was sourced mainly in coeval igneous rocks.

4.3.4 Hf Model ages of the three studied sections

The compilation of the Hf TDM_2 model ages obtained for the analysed Permian and Triassic zircons and inherited cores in the three investigated sections yield a main peak at ca. 1.57 Ga (Fig. 6d) within a range between 2.5 and 0.7 Ga. One outlier shows ca. 3.35 Ga. These results are consistent with Hf TDM_2 model ages obtained in zircons from pre-Alpine basement rocks in the Penninic domain and Alpine detrital zircons, which range between 2.5 and 0.6 Ga with a main peak at ca. 1.55 Ga (Beltrán-Triviño et al. in preparation). Furthermore, Schaltegger and Gebauer (1999) and references therein, presented Nd and Hf model ages of granites from the Alpine basement of 1.5–1.6 Ga, documented older components in the Austroalpine Silvretta basement by model ages ranging between 1.9 and 1.7, and reported that the addition of subcontinental mantle-derived magmas to old crust (e.g. 1.7 Ga) might produce model ages at around 1.3–0.9.

These considerations allow us to observe that the Permian and Triassic magmatism in the South-Alpine and Austroalpine domains have a common range of model ages together with elements of the Palaeozoic basement of the Penninic and Helvetic domains. Although differences in model ages are due to mixing of different source composition and they do not signify geological events, it is remarkable that our model age range matches the timing of the Proterozoic mantle mobilization events at ca. 1.7–1.6 and 1.3–0.8 Ga postulated by Schulz (2008).

4.4 Single mineral composition

4.4.1 Feldspars

Trevena and Nash (1979, 1981) compiled a large database of the composition of plagioclases from igneous and metamorphic rocks. They proposed seven groups for the provenance of detrital plagioclases. We assume that the analysed feldspars are part of the primary sedimentary cycle and therefore, mirror the original source. The zircon age distributions indicate that the Dasdana beds and Bellano Fm were supplied from Early Permian magmatic products (Fig. 4b, c), and that the Buchenstein Fm and Val Sabbia Sst. (Fig. 4b) were mainly sourced by Middle Triassic magmatic rocks. The variation of feldspar compositions determined by electron microprobe in the Southalpine Early Permian Dasdana beds (VT2), the Anisian Bellano Fm (10AB03), the Ladinian volcaniclastic horizon in the Buchenstein Fm (PBFT11) and the Carnian Val Sabbia Sst. (10AB08) is depicted in Fig. 7.

According to modal grain counting, the Permian Dasdana beds sample (VT2) comprises sub-angular crystal fragments of plagioclase (35%), K-feldspar (25%), quartz (25%), volcanic (5%) and sedimentary lithics (5%), and biotite (5%). The Dasdana feldspars yield two well-defined groups, both with very low-Ca contents. Plagioclases with high-Na (albite end-member) predominate quantitatively over K-feldspar (Fig. 7). Generally, albite end-member of the plagioclase series is correlated with a large variety of source rocks such as granites, granite-pegmatites, alkali-diorites, basalts, and also with authigenic processes. According to the classification of Trevena and Nash (1979, 1981), the high-Na plagioclases fall in the plutonic–low-rank metamorphic-authigenic fields. K-feldspar is a common mineral in granites, syenites, and pegmatites, but also in rapid-cooling volcanics and felsic pyroclastics.

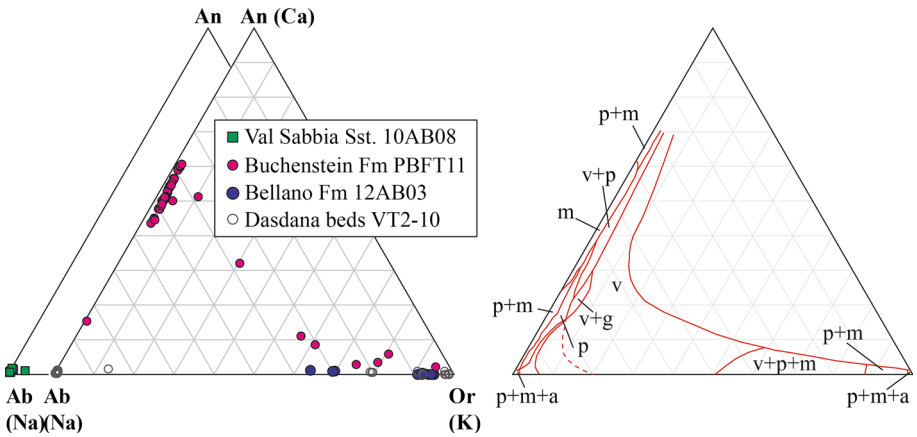

Fig. 7 Left: ternary diagram showing compositional variation of feldspars using electron microprobe. *An* anorthite, *Ab* albite, *Or* orthoclase. Right: diagram showing compositional range of eight provenance group of feldspars, *v* volcanic, *p* plutonic, *m* metamorphic, *g* granophyre, *a* authigenic

Sample 12AB03 from the Anisian Bellano Fm is a feldspathic litharenite, which contains subangular crystal fragments of quartz (30%), feldspars (20%), volcanic lithics (40%), sedimentary lithics (10%) and biotite. The feldspars show low-Ca and high-K (orthoclase end-member >60%) compositions (Fig. 7), indicating a volcanic-plutonic origin.

The volcaniclastic horizon in the upper part of the Buchenstein Formation (PBFT11) delivered phenocrysts of quartz (10%), feldspar: plagioclase and minor K-feldspar (20%), sedimentary (20%) and volcanic lithics (45%), and biotite (5%). The analysed feldspars with low-K, high-Ca and high-Na (Fig. 7) suggest a volcanic–plutonic provenance. The plagioclases can be distinguished from metamorphic plagioclases because the orthoclase content of volcanic plagioclase increases with decreasing anorthite component (Trevena and Nash 1979, 1981; Fig. 7).

The sample from the Carnian Val Sabbia Sst. (10AB08) is a litharenite that comprises sub-angular crystal fragments of quartz (30%), feldspar (10%) and lithic volcanic fragments (60%). Similarly to the Dasdana beds sample, the composition of the plagioclases is very low-Ca and very high-Na, and falling in the plutonic–low-rank metamorphic-authigenic field.

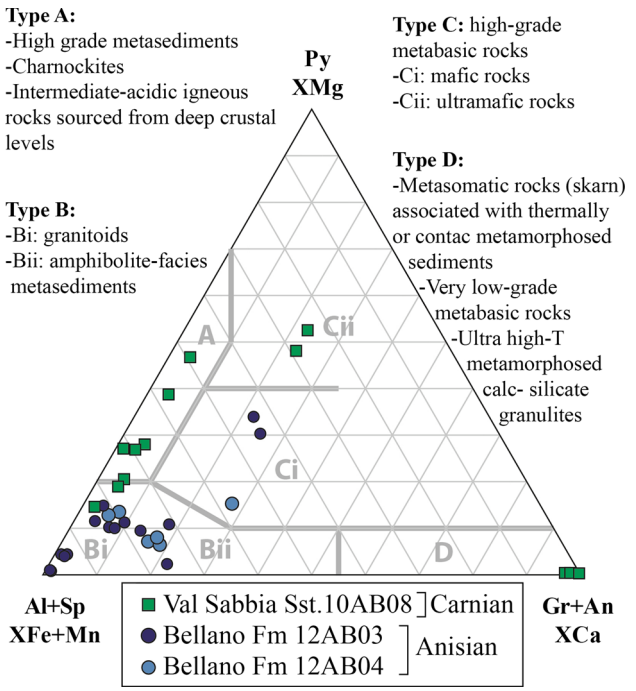

Fig. 8 Ternary diagram showing compositional variation of garnets using electron microprobe; *Py* pyrope, *Al* almandine, *Sp* spessartine, *Gr* grossular, *An* andradite. The boundaries of the compositional fields (A, Bi, Bii, Ci, Cii and D) and their probable provenance were taken from Mange and Morton (2007)

4.4.2 Heavy minerals: garnet and chromian spinel

Detrital garnet geochemistry is a widely used technique for determination and discrimination of sedimentary provenance. We assume that the analysed grains are detrital garnets which are part of the primary sedimentary cycle. The variations in garnet composition from the Bellano Fm and Val Sabbia Sst. are shown into a discrimination scheme of garnet types (Fig. 8). This classification is based on the Fe + Mn–Mg–Ca composition of the garnets, and it assigns to each garnet type possible source rocks. This scheme is based on modern and ancient sediments (Mange and Morton 2007). Most of the garnets from the Anisian Bellano Fm (ca. 80%), fall in the Type Bi field with low-Ca ($X_{Ca} < 10\%$) and high-Mn, suggesting an origin from granitoids and/or intermediate-acidic igneous rocks. With respect to the detrital zircon ages (Fig. 4c), these sources might include rocks associated with the Permian magmatic rocks of the Southern Alps (see peak in Fig. 4c). The garnets in the Bii field indicate a source in amphibolite facies metasediments, and the detrital zircon record suggest that the sources are presumably related with Pre-Variscan, likely Ordovician, basement rocks (see peak in Fig. 4c) of the northwestern part of the Southern Alps.

Some garnets from the same formation fall in the Type Ci field ($X_{Mg} < 40\%$), which implies that these garnets might be derived from mafic rocks. They presumably are derived from mafic intrusions as the Mafic Complex in the Ivrea-Verbano Zone (IVZ) in the westernmost part of the Southern Alps. These rocks are coeval with, and genetically related with granitic bodies in the middle to upper crust and explosive, rhyolitic volcanism within the so-called Serie dei Laghi in the western Southern Alps (Schaltegger and Brack 2007).

Based on the same classification scheme, most of the garnets from the Carnian Val Sabbia Sst. fall in the Type A field (Fig. 8), suggesting an origin from high-grade (granulite facies) metasedimentary rocks or charnockites. However, this contrasts with the absence of metamorphic lithic clasts or diagnostic metamorphic minerals in the sandstone detritus. Moreover, Type A garnets also have been reported from xenocrysts or in xenoliths in intermediate-acidic igneous rocks, representing material incorporated into the magma at deep crustal levels (Hamer and Moyes 1982). Two garnets plot at the boundary of Type A and Bi, and one garnet falls entirely in the Bi field, indicating an origin in granitoids and/or intermediate-acidic igneous rocks. Two garnets with $X_{Mg} > 40\%$ plot in the Type Cii field, indicating a derivation from ultramafic igneous rocks, which might evidence the incorporation of mantle-related material into the magma at the lower crust or the upper mantle levels.

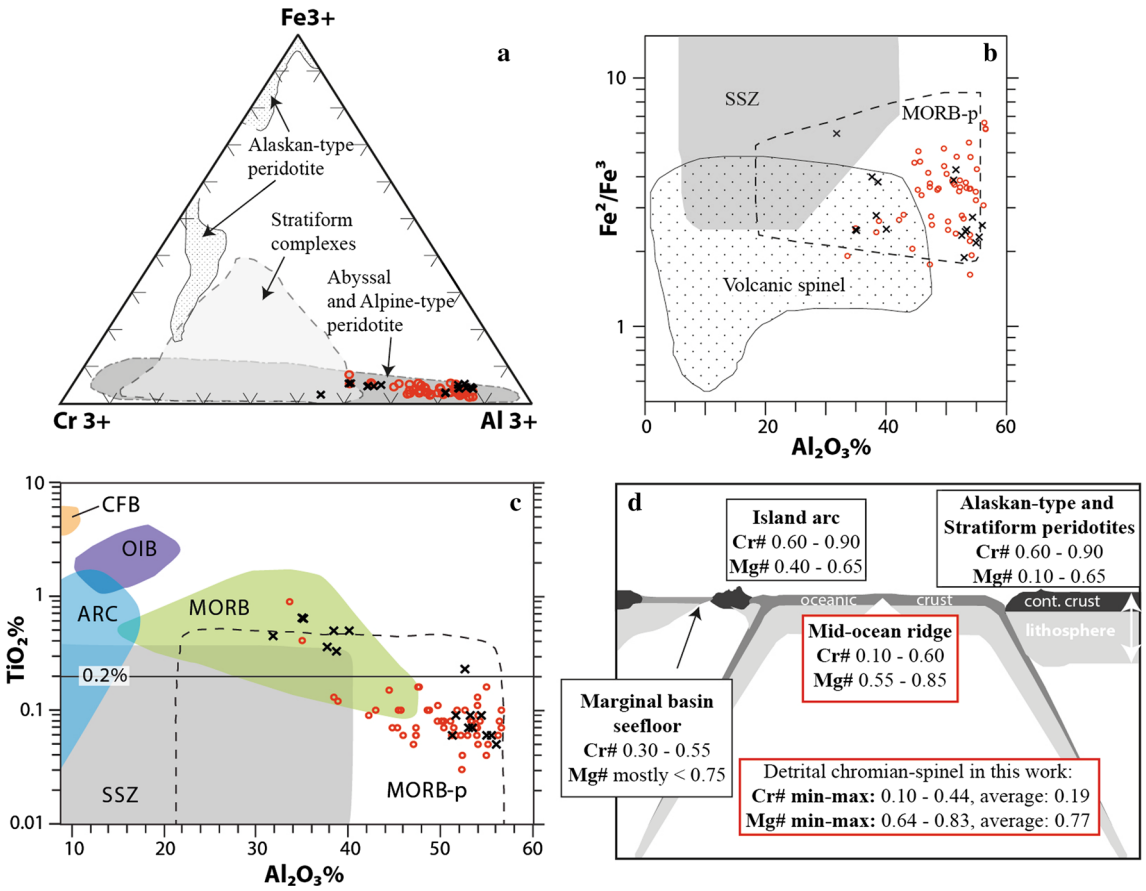

Fig. 9 Detrital chromian spinel compositional variation diagrams of the Val Sabbia Ss. Red circles represent translucent grains and black crosses represent opaque grains: **a** Ternary plot of the major trivalent cations in chromian spinel. Fields compiled by Cookenboo et al. (1997) and references therein: i) Alaskan-type; ii) Stratiform field shows compositional range of spinels in ultramafic bodies produced by fractional crystallisation in the crust; iii) Abyssal and Alpine-type peridotites field includes chromian spinel of mantle melting origin as ultramafic xenoliths, abyssal dunites, spinel-plagioclase peridotites and Alpine-type peridotites. **b** Discrimination between volcanic and mantle spinel using Al_2O_3 and Fe^{2+}/Fe^{3+} values. SSZ: suprasubduction zone; MORB-p: Mid-ocean ridge-type peridotites (Kamenetsky et al. 2001). **c** Spinel field diagram Al_2O_3 vs TiO_2; ARC: arc; CFB: continental flood basalts; MORB: mid-ocean ridge basalts; MORB-p: MORB-type peridotites; OIB: oceanic island basalts; SSZ: suprasubduction zone (fields from Kamenetsky et al. 2001, and Hu et al. 2014). **d** Typical spinel compositions from various sea-floor and continental crust origin. No scale implied. Modified from Cookenboo et al. (1997). See detailed compositional diagrams in the Online Resource 5

In summary, the variation of the garnet composition from type-B and Ci in the Anisian Bellano Fm in the Western Lombardy section to type-A and Cii in the Carnian Val Sabbia Sst. in the Eastern Lombardy section (Fig. 8), indicate different source areas during the Middle Triassic in the South-Alpine domain. The Bellano Fm was presumably sourced in Ordovician metasediments or its sedimentary cover, and in Permian intermediate-acidic igneous rocks, probably with lower crust xenoliths, or Permian mafic rocks associated to the Mafic Complex of the IVZ during the Anisian stage. During the Carnian, the Val Sabbia Sst. was probably sourced in Middle Triassic intermediate-acidic igneous rocks with lower crust xenoliths. The mafic–ultramafic xenoliths are presumably associated with the Middle Triassic Finero mafic intrusion emplaced in the IVZ (Zanetti et al. 2013).

Chromian spinel is a good petrogenetic indicator due to its chemical character, which is sensitive to bulk rock composition and petrogenesis of the host rock. The variation of the chemical composition of Cr-rich spinel represents the magma chemistry (Arai 1992, 1994). Different compositional diagrams of chromian spinel from the Val Sabbia Sst. (Fig. 9a–c) allow us to discriminate an origin associated with MORB-type peridotites rather than volcanic, due to their low content of Cr^{3+} and Fe^{3+} and the high concentration of Al_2O_3. The values of Cr and Mg atomic numbers (Cr# and Mg# in Fig. 9d) suggest an origin associated with a mid-ocean-ridge setting.

Furthermore, the ratios of Cr# and Mg# (Online Resource 5) suggest that chromian spinel of the Val Sabbia Sst.: (1) is derived from abyssal peridotites and/or xenoliths from basalts, (2) lies in the compositional field of

lherzolites, and (3) shows affinity with Type-I Alpine-type peridotites. According to Dick and Bullen (1984) these combined results suggest that the origin of the chromian spinel might be related to a section of oceanic lithosphere formed at a mid-ocean ridge.

The interpretations of garnet (Fig. 8) and chromian spinel geochemistry of the Val Sabbia Sst. (Figs. 8, 9; Online Resource 5) support each other. These heavy minerals indicate the presence of mafic and ultramafic rocks exposed in the Southalpine domain at the Carnian age. Most probably they were supplied from mantle xenoliths observed in the intermediate-acidic Middle Triassic volcanic rocks of the Southern Alps (pers. comm. Peter Brack). Upper mantle lherzolite xenoliths in the Triassic igneous complex of Predazzo are reported in the central Southern Alps (Carraro and Visona 2003). Furthermore, Zanetti et al. (2013) propose that the intrusion of the Finero Mafic Complex at the IVZ may represent a deep-crustal counterpart of the Middle Triassic volcanism that is widespread throughout the Southern Alps. These lower crust and upper mantle elements are comparable with our detrital garnet and chromian spinel data set.

5 Interpretations of the Permian and Triassic magmatism in the South-Alpine and Austroalpine domains

5.1 Early Permian magmatism

It is generally accepted that during the Early Permian in the Southern Alps, post-Variscan intracontinental extension and strike-slip tectonics controlled basin formation, and the related magmatism was sourced in mixed mantle-crust magmas (e.g. Schaltegger and Brack 2007). According to this model, basin formation and magmatism occurred in a short time span between 285 and 275 Ma. This crustal magmatism involving mantle and crust sources was a widespread episode recognised in both the South-Alpine and the Austroalpine domains (e.g. Spalla and Gosso 2002, Schaltegger and Brack 2007 and references therein).

Published data from the IVZ and Serie dei Laghi in the Southern Alps documented that intrusion of mafic magma began at ca. 314 Ma and continued, episodically, for more than 30 My concluding in the major Permian magmatic stage that assembled an 8-km-thick mafic complex in the deep crust, large granitic plutons in the upper crust, and volcanism between ca. 290 and 280 Ma (Klötzli et al. 2014). Coeval with the cessation of magmatic activity, clastic sedimentation ceased at ca. 275 Ma. This is recorded by the Middle Permian unconformity, which represents a time gap of ca. 10 Ma (Gretter et al. 2013). This period correlates with the model of the transition from Early Permian Pangaea A to Late Permian Pangaea B, due to the activation of a regional scale dextral displacement fault along reactivated late Variscan shear zones (Muttoni et al. 2003).

The peak of the Early Permian magmatism is documented by the U–Pb detrital zircon age distribution of the Austroalpine Fuorn and Saluver formations (Fig. 4a) at ca. 290 Ma. This age matches with the magmatic activity between ca. 295-288 Ma reported from Austroalpine basement units (e.g. von Quadt et al. 1994). The U–Pb age patterns in the South Alpine Dasdana beds (Fig. 4b) and Bellano Fm (Fig. 4c) reveal a peak at ca. 280 Ma, which coincides with the previously proposed period of basin formation and magmatism between 285 and 275 Ma along an E-W transect on the Southern Alps (Schaltegger and Brack 2007) and in the Athesian volcanic group in the eastern Southern Alps (Marocchi et al. 2008). For further comparison, a bimodal magmatic phase occurred at around 285 Ma in the Permian Glarus Verrucano basin situated in the later Helvetic palaeogeographic domain (Letsch et al. 2015).

Our estimated εHf(t) values for the Permian zircons from the Austroalpine Fuorn and Saluver formations (Fig. 5a), the South-Alpine Dasdana beds (Fig. 5b) and the Bellano Fm (Fig. 5c) cluster between −8 and −1, with sparse positive values. These results are in perfect agreement with Hf isotopic analyses of Permian magmatic rocks in the South-Alpine domain (Schaltegger and Brack 2007) and in the South-Alpine, Penninic and Helvetic realms (Stille and Steiger 1991). Similar recent analyses of εHf(t) on detrital zircons of the Glarus Verrucano revealed a main cluster between −4 and −8 (Letsch et al. 2015). These results support our model of mixing of mantle with predominance of recycled crustal components in the melts of the Early Permian magmatism. Finally, the occurrence of Type Ci garnet in the Bellano Fm (Fig. 8) suggests the incorporation of mantle-derived material into the magmas at deep crustal level. This interpretation is in line with previous results (e.g. Rottura et al. 1998) suggesting the hybrid nature of the Early Permian melts with the participation of mantle melts in the generation of acidic and intermediate intrusions.

5.2 Middle Triassic magmatism

The geodynamic significance of the Middle Triassic magmatic episodes is still a matter of debate, mainly because the geodynamic evolution of the South-Alpine and Austroalpine terranes during Permian–Triassic period is not yet well understood. The intricate Late Palaeozoic geodynamic evolution encompasses the transition from the Variscan to the Alpine orogenic cycle. In particular, Triassic magmatic signatures play a crucial role in the interpretation of the tectonic evolution.

Contrasting tectono-magmatic models for the Middle Triassic magmatism in the Southern Alps were proposed, among others: (1) volcanism related to aborted rifting stages (Ferrara and Innocenti, 1974), (2) magmatism within a marginal back-arc basin associated with the post-Variscan evolution of the Alpine sector (Marinelli et al. 1980, in Crisci et al. 1984), (3) subduction-related arc magmatism associated with the foundering of the lower continental crust in the upper mantle (Castellarin et al. 1980, 1988), (4) magmatism associated with partial melting in the upper mantle, which had been hydrated and modified during the preceding Variscan orogenesis and contaminated by the incorporation of large portions of crustal material (Crisci et al. 1984), (5) magmatism in an epicontinental arc or back-arc setting driven by the northward subduction of remnants of the Palaeothetys ocean (Garzanti 1985, 1986; Stampfli et al. 2002), and (6) Ladinian magmatism (ca. 232 Ma) in the IVZ related to extensional tectonics in the lower crust, which concurs with a 230–180 Ma high-T shear zone (Zanetti et al. 2013, and references therein).

As described previously, Middle and early Late Triassic sequences contain volcaniclastic and pyroclastic horizons. Detrital zircons derived from selected basins (Figs. 1, 3) reveal magmatic activity at ca. 244–243 Ma in the Eastern Alps (Fig. 4a) and ca. 240–237 Ma (Fig. 4b–c) in the Southern Alps. Our age ranges compare well with previously published high-precision ages in the Southern Alps (Mundil et al. 1996; Brack et al. 2007) and in the Eastern Alps (Furrer et al. 2008) (see compilation in Fig. 3).

According to the presented data, the magma sources of the Middle Triassic magmatism originated from mixing crustal and mantle components. The εHf(t) of the Middle Triassic zircons from the Austroalpine Prosanto Fm are positive, ca. 0 to +10 (Fig. 5a), indicating a mantle derived magma with minor crustal contamination. In contrast, the Middle Triassic zircons from the Austroalpine Altein Fm (Fig. 5a), and the South-Alpine Buchenstein Fm, Val Sabbia Sst. (Fig. 5b) and Meride Lmst. (Fig. 5c) are dominated by negative values −10 to +4, suggesting higher influence of crustal components in the melts. The Austroalpine Prosanto zircons exhibit a more juvenile signature than the others, presumably due to the augmented incorporation of mantle material into the magma. In considering the Hf TDM_2 model ages as a hybrid age of the magma components, the younger crustal residence time observed in the Prosanto Fm (Fig. 6a) corroborates the addition of the juvenile material and consequently, a decrease of the hybrid age of the magma source.

Primarily, the occurrence of Type Bi garnets in the South-Alpine Carnian Val Sabbia Sst. (Fig. 8) is in line with the provenance from intermediate to acidic igneous rocks. However, the presence of Type A and Cii garnets suggests the incorporation of mantle components into the melts at deep crustal levels. In addition, Type D garnet in the Val Sabbia Sst. might be an indicator of low-grade metasomatism of the underlying Ladinian carbonate platforms; however, our dataset is too sparse for testing this.

Previous zircon Hf-isotope based investigations in ancient volcanic arc settings show a high dispersion of the εHf(t), with a predominance of positive values within the same crystallisation-age interval, similar to that found in the Carboniferous-Permian Gobi volcanic belt in northern Mongolia (Bussien et al. 2011) and the Middle Triassic Gangcha complex in Central China (Guo et al. 2012). The rather low dispersion of the predominating negative εHf(t) values in our dataset do not corroborate volcanic arc magmatism. On the contrary, our εHf(t) results are consistent with those values obtained from asthenospheric upwelling, as has been described in a Permian–Triassic post-collisonal extensional setting, at the northern margin of the North China continental block (Bai et al. 2013). Moreover, it has been suggested for western Mediterranean Triassic rift-basins that calc-alkaline geochemical signature of intermediate to acidic magmatism is not necessarily an indicator of subduction-related magmatism, and instead this geochemical signature might be a lithosphere-hosted inheritance from the previous Variscan subduction (Dixon and Robertson 1993; Robertson 2006).

The εHf(t) values of the Triassic zircons from the Southern and Eastern Alps are slightly higher than the estimated for the Permian zircons (Fig. 5). This observation suggests an evolution in mixing mantle and crustal components into the melts within an extensional and strike-slip tectonic setting, as interpreted for the Permian continental crust of the Southern Alps by Schaltegger and Brack (2007). The Hf-signatures of the Triassic zircons show a lower influence of crust components into the parental magma-mix than observed in the Permian crystals, which we interpreted as shown in Fig. 10, as progressive mantle rising and exhumation during continue extension and thinning of the lithospheric crust due to the initial rifting process, probably asymmetric, of the Alpine Tethys oceanic system. We speculate that if the Permian melts have a crustal component of 50–55%, the Triassic melts might have reached 45–50% of crustal components.

The Middle Permian unconformity, which separates the Early Permian lacustrine sediments and magmatic products from the Late Permian–Early Triassic non-volcanic deposits, does not suggest a regional modification of the tectono-magmatic environment. In contrast, it rather documents a local short-lived Middle Permian compressive phase (Cassinis et al. 2012) that caused the deposition of Late Permian fluvial facies in the western Southern Alps (Gretter et al. 2013).

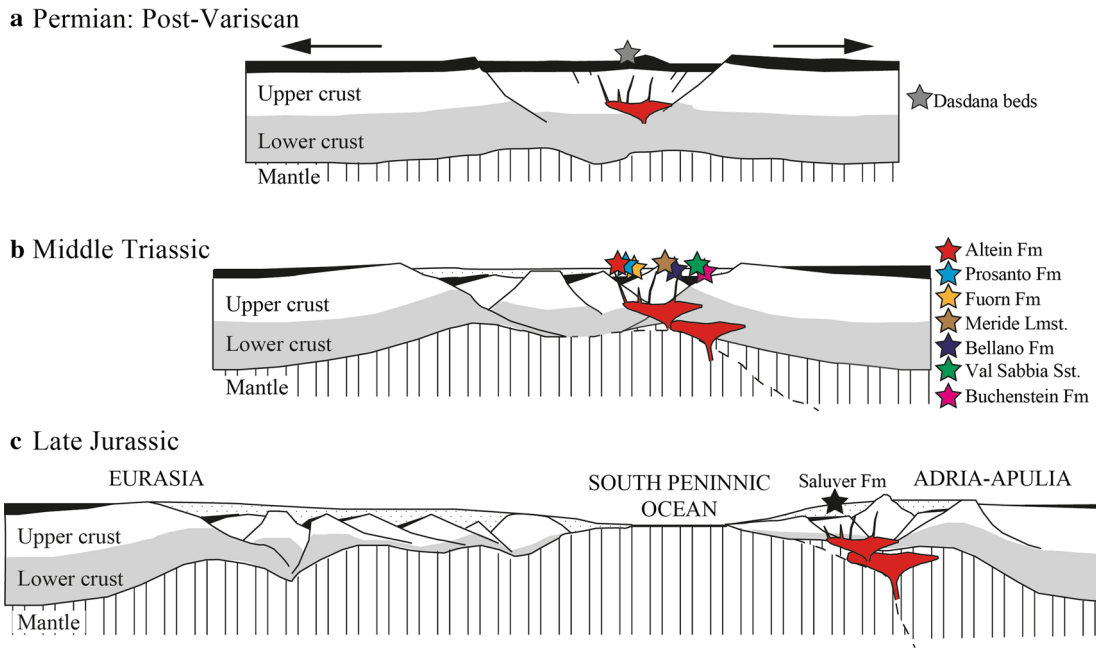

Fig. 10 Sketch (not to scale) of the tectonic interpretation during the Permian and Triassic magmatic events, and during the Jurassic oceanic crust formation. The stars indicate the possible position of the analysed units. The orientation of the profiles is shown in the palaeogeographic map in Fig. 2b

The complete source characteristics of the Middle Triassic magmatism in the Southern and Eastern Alps document continued melting of Variscan and older continental crust, and incorporation of mantle components at deep crustal levels, within an inherited post-Variscan extensional to strike-slip tectonic setting. Progressive lithospheric extension and thinning, and mantle upwelling operating since the Permian, most likely have driven the Triassic intracontinental rift process, which marks the onset of the Jurassic opening of the Alpine Tethys oceanic domain.

6 Conclusions

1. The South-Alpine Early Permian Dasdana beds in the Eastern Lombardy section were sourced by local syn-depositional magmatic activity.
2. The Austroalpine and South-Alpine Middle Triassic basins were sourced mainly in coeval igneous rocks. The Anisian South-Alpine Bellano Fm and the Austroalpine Fuorn Fm were sourced additionally in Early Permian igneous or volcaniclastic (Verrucano-type) rocks, and post-Cadomian basement units.
3. Permian (post-Variscan) and Triassic (early-Alpine) partial melting of older continental crusts is documented by the presence of post-Variscan, Variscan and older inherited cores in the detrital zircons.
4. The initial Hf-isotopic compositions confirm that Permian and Triassic melts had similar mixed mantle-crust magma sources, with lower influence of crust material in the Triassic melts. This evolution is compatible with a progressive extension and thinning of the continental crust, probably associated with the Pangaea break-up.
5. The Triassic magmas formed through partial melting in the upper mantle and lower crust. The magma sources were deeply modified during the preceding Variscan orogeny. Therefore, the Triassic melts inherited the calc-alkaline signature of the Variscan compressional setting.
6. Hf-depleted mantle two-stage model ages obtained in Palaeozoic inherited cores and in Permian and Triassic zircons clustered around 1.7–1.5 Ga, indicating a common hybrid age of the sources of the Permian and Triassic magmatism.
7. We propose that post-Variscan transtension and Triassic rifting represent a joint and long-lasting process of continental Pangaea break-up in the Alpine Tethys. Our interpretation of the results allow us to propose extension-related magmatism during the Middle Triassic in the Southern and Eastern Alps rather than subduction-related magmatic activity suggested by previous studies.

Acknowledgements Peter Brack is gratefully acknowledged for providing samples from Dasdana beds and Buchenstein Fm, for

helpful assistance in the field and for fruitful discussions on the Permian–Triassic evolution of the Southern Alps. We thank Hans Furrer for providing samples from Prosanto and Altein formations and profitable discussions on the Middle Triassic stratigraphy of the Eastern Alps. Advising on the Lu–Hf systematics by P. Sprung is widely appreciated. D. Hunziker, J. von Rütte and A. Mohammadi provided invaluable laboratory assistance. We also thanks to S. Scott for improve the English language of the manuscript. The comments and suggestions from two anonymous reviewers are highly appreciated. This work was supported by an ETH Zurich internal Grant No. 04 09-1.

References

Amelin, Y., Lee, D. C., Halliday, A. N., & Pidgeon, R. T. (1999). Nature of the Earth's earliest crust from hafnium isotopes in single detrital zircons. *Nature, 399*, 252–255.

Arai, S. (1992). Chemistry of Chromian spinel in volcanic-rocks as a potential guide to magma chemistry. *Mineralogical Magazine, 56*, 173–184.

Arai, S. (1994). Characterization of spinel peridotites by olivine spinel compositional relationships—review and interpretation. *Chemical Geology, 113*, 191–204.

Augustsson, C., Munker, C., Bahlburg, H., & Fanning, C. M. (2006). Provenance of late Palaeozoic metasediments of the SW South American Gondwana margin: a combined U–Pb and Hf-isotope study of single detrital zircons. *Journal of the Geological Society, 163*, 983–995.

Bahlburg, H., Vervoort, J. D., DuFrane, S. A., Carlotto, V., Reimann, C., & Cardenas, J. (2011). The U-Pb and Hf isotope evidence of detrital zircons of the Ordovician Ollantaytambo Formation, southern Peru, and the Ordovician provenance and paleogeography of southern Peru and northern Bolivia. *Journal of South American Earth Sciences, 32*, 196–209.

Bai, X., Liu, S. W., Wang, W., Yang, P. T., & Li, Q. G. (2013). U-Pb geochronology and Lu-Hf isotopes of zircons from newly identified Permian-Early Triassic plutons in western Liaoning province along the northern margin of the North China Craton: constraints on petrogenesis and tectonic setting. *International Journal of Earth Sciences, 102*, 671–685.

Beltrán-Triviño, A., Winkler, W., & Von Quadt, A. (2013). Tracing Alpine sediment sources through laser ablation U-Pb dating and Hf-isotopes of detrital zircons. *Sedimentology, 60*, 197–224.

Bertotti, G., Picotti, V., Bernoulli, D., & Castellarin, A. (1993). From Rifting to drifting—tectonic evolution of the South-Alpine upper crust from the Triassic to the early cretaceous. *Sedimentary Geology, 86*, 53–76.

Bodet, F., & Schärer, U. (2000). Evolution of the SE-Asian continent from U-Pb and Hf isotopes in single grains of zircon and baddeleyite from large rivers. *Geochimica et Cosmochimica Acta, 64*, 2067–2091.

Bouvier, A., Vervoort, J. D., & Patchett, P. J. (2008). The Lu-Hf and Sm-Nd isotopic composition of CHUR: Constraints from unequilibrated chondrites and implications for the bulk composition of terrestrial planets. *Earth and Planetary Science Letters, 273*, 48–57.

Brack, P., Rieber, H., Mundil, R., Blendinger, W., & Maurer, F. (2007). Geometry and chronology of growth and drowning of Middle Triassic carbonate platforms (Cernera and Biviera/Clapsavon) in the Southern Alps (northern Italy). *Swiss Journal of Geosciences, 100*, 327–347.

Breitkreuz, C., Cortesogno, L., & Gaggero, L. (2002). Crystal-rich mass flow deposits related to the eruption of a sublacustrine silicic cryptodome (Early Permian Collio Basin, Italian Alps). *Journal of Volcanology and Geothermal Research, 114*, 373–390.

Bussien, D., Gombojav, N., Winkler, W., & von Quadt, A. (2011). The Mongol-Okhotsk Belt in Mongolia—an appraisal of the geodynamic development by the study of sandstone provenance and detrital zircons. *Tectonophysics, 510*, 132–150.

Carraro, A., & Visona, D. (2003). Mantle xenoliths in Triassic camptonite dykes of the Predazzo Area (Dolomites, Northern Italy): petrography, mineral chemistry and geothermobarometry. *European Journal of Mineralogy, 15*, 103–115.

Cassinis, G., Cortesogno, L., Gaggero, L., Perotti, C., & Ronchi, A. (2007). Volcanic products from the Early Permian Collio Basin (southern Alps) and their geodynamic implications. *Periodico Di Mineralogia, 76*, 25–47.

Cassinis, G., Cortesogno, L., Gaggero, L., Perotti, C. R., & Buzzi, L. (2008). Permian to Triassic geodynamic and magmatic evolution of the Brescian Prealps (eastern Lombardy, Italy). *Bollettino Della Societa Geologica Italiana, 127*, 501–518.

Cassinis, G., Perotti, C. R., & Ronchi, A. (2012). Permian continental basins in the Southern Alps (Italy) and peri-mediterranean correlations. *International Journal of Earth Sciences, 101*, 129–157.

Castellarin, A., Lucchini, F., Rossi, F., Simboli, G., Bosellini, A., & Somavilla, E. (1980). Middle Triassic magmatism in the Southern Alps. II. A geodynamic model. *Rivista Italiana di Paleontologia e Stratigrafia, 85*, 1111–1124.

Castellarin, A., Lucchini, F., Rossi, P. L., Selli, L., & Simboli, G. (1988). The Middle Triassic magmatic-tectonic arc development in the Southern Alps. *Tectonophysics, 146*, 79–89.

Cohen, K. M., Finney, S. C., Gibbard, P. L., & Fan, J. X. (2013). The ICS International Chronostratigraphic Chart. *Episodes, 36*, 199–204.

Cookenboo, H. O., Bustin, R. M., & Wilks, K. R. (1997). Detrital chromian spinel compositions used to reconstruct the tectonic setting of provenance: Implications for orogeny in the Canadian cordillera. *Journal of Sedimentary Research, 67*, 116–123.

Crisci, C. M., Ferrara, G., Mazzuoli, R., & Rossi, P. M. (1984). Geochemical and geochronological data on Triassic volcanism of the Southern Alps of Lombardy (Italy)-genetic implicaitons-. *Geologische Rundschau, 73*, 279–292.

Dick, H. J. B., & Bullen, T. (1984). Chromian spinel as a petrogenetic indicator in Abyssal and Alpine-Type peridotites and spatially associated lavas. *Contributions to Mineralogy and Petrology, 86*, 54–76.

Dixon, J. E., & Robertson, A. H. F. (1993). Arc signatures in Mediterranean Triassic rift basalts: a lithosphere-hosted inheritance from Hercynian subduction. *Terra Nova, 5*(Suppl. 1), 424.

Dössegger, R. (1974). Verrucano und "Bundsandstein" in den Unterengadiner Dolomiten. PhD Dissertation, ETH Zürich, Zürich, pp. 171.

Ferrara, G., & Innocenti, F. (1974). Radiometric age evidences of a Triassic Thermal Event in the Southern Alps. *Geologische Rundschau, 63*, 572–581.

Furrer, H. (1985). Field Workshop on Triassic and Jurassic Sediments in the Easten Alps of Switzerland (Vol. 248, pp. 81). Zürich: Mitteilungen Geologisches Institut der ETH und Universität Zürich.

Furrer, H. (1995). The Kalkschieferzone (Upper Meride Limestone; Ladinian) near Meride (Canton Ticino, Southern Switzerland) and the evolution of a Middle Triassic intraplatform basin. *Eclogae Geologicae Helvetiae, 88*, 827–852.

Furrer, H., Schaltegger, U., Ovtcharova, M., & Meister, P. (2008). U-Pb zircon age of volcaniclastic layers in Middle Triassic platform carbonates of the Austroalpine Silvretta nappe (Switzerland). *Swiss Journal of Geosciences, 101*, 595–603.

Garzanti, E. (1985). The sandstone memory of the evolution of a Triassic volcanic arc in teh Southern Alps, Italy. *Sedimentology, 32*, 423–433.

Garzanti, E. (1986). Source rock versus sedimentary control on the mineralogy of deltaic volcanic arenites (Upper Triassic, Northern Italy). *Journal of Sedimentary Petrology, 56*, 267–275.

Gretter, N., Ronchi, A., Langone, A., & Perotti, C. R. (2013). The transition between the two major Permian tectono-stratigraphic cycles in the central Southern Alps: Results from facies analysis and U/Pb geochronology. *International Journal of Earth Sciences, 102*, 1181–1202.

Griffin, W. L., Pearson, N. J., Belousova, E., Jackson, S. E., van Achterberg, E., O'Reilly, S. Y., et al. (2000). The Hf isotope composition of cratonic mantle: LAM-MC-ICPMS analysis of zircon megacrysts in kimberlites. *Geochimica et Cosmochimica Acta, 64*, 133–147.

Griffin, W. L., Wang, X., Jackson, S. E., Pearson, N. J., O'Reilly, S. Y., Xu, X., et al. (2002). Zircon chemistry and magma mixing, SE China: In-situ analysis of Hf isotopes, Tonglu and Pingtan igneous complexes. *Lithos, 61*, 237–269.

Guo, X. Q., Yan, Z., Wang, Z. Q., Wang, T., Hou, K. J., Fu, C. L., et al. (2012). Middle Triassic arc magmatism along the northeastern margin of the Tibet: U-Pb and Lu-Hf zircon characterization of the Gangcha complex in the West Qinling terrane, central China. *Journal of the Geological Society, 169*, 327–336.

Hamer, R. D., & Moyes, A. B. (1982). Composition and Origin of Garnet from the Antarctic Peninsula Volcanic Group of Trinity Peninsula. *Journal of the Geological Society, 139*, 713–720.

Hu, X., An, W., Wang, J., Garzanti, E., & Guo, R. (2014). Himalayan detrital chromian spinels and timing of Indus-Yarlung ophiolite erosion. *Tectonophysics, 621*, 60–68.

Iizuka, T., Komiya, T., Rino, S., Maruyama, S., & Hirata, T. (2010). Detrital zircon evidence for Hf isotopic evolution of granitoid crust and continental growth. *Geochimica et Cosmochimica Acta, 74*, 2450–2472.

Jackson, S. E., Pearson, N. J., Griffin, W. L., & Belousova, E. A. (2004). The application of laser ablation-inductively coupled plasma-mass spectrometry to in situ U-Pb zircon geochronology. *Chemical Geology, 211*, 47–69.

Kamenetsky, V., Crawford, A. J., & Meffre, S. (2001). Factors controlling chemistry of magmatic spinel: an empirical study of associated olivine, Cr-spinel and melt inclusions from primitive rocks. *Journal of Petrology, 42*, 655–671.

Letsch, D., Winkler, W., von Quadt, A., & Gallhofer, D. (2015). The volcano-sedimentary evolution of a post-Variscan intramontane basin in the Swiss Alps (Glarus Verrucano) as revealed by zircon U-Pb age dating and Hf isotope geochemistry. *International Journal of Earth Sciences, 104*, 123–145.

Ludwig, K. (2012). User's Manual for Isoplot 3.75 A Geochronological Toolkit for Microsoft Excel (Vol. 5, pp. 75). Berkeley: Berkeley Geochronology Center Special Publication.

Mange, M. A., & Maurer, H. F. W. (1992). Heavy Minerals in Colour (pp. 147). London: Chapman and Hall.

Mange, M. A., & Morton, A. C. (2007). Geochemistry of heavy minerals. In M. A. Mange & D. Wright (Eds.), *Heavy Minerals in use: Developments in Sedimentology* (Vol. 58, pp. 345–391): Elsevier. doi:10.1016/S0070-4571(07)58013-1

Marocchi, M., Morelli, C., Mair, V., Klotzli, U., & Bargossi, G. M. (2008). Evolution of large silicic magma systems: New U-Pb zircon data on the NW Permian Athesian Volcanic Group (Southern Alps, Italy). *Journal of Geology, 116*, 480–498.

Matteini, M., Dantas, E. L., Pimentel, M. M., & Buhn, B. (2010a). Combined U-Pb and Lu-Hf isotope analyses by laser ablation MC-ICP-MS: methodology and applications. *Anais Da Academia Brasileira De Ciencias, 82*, 479–491.

Matteini, M., Junges, S. L., Dantas, E. L., Pimentel, M. M., & Buhn, B. (2010b). In situ zircon U-Pb and Lu-Hf isotope systematic on magmatic rocks: Insights on the crustal evolution of the Neoproterozoic Goias Magmatic Arc, Brasilia belt, Central Brazil. *Gondwana Research, 17*, 1–12.

McCann, T., Pascal, C., Timmerman, M. J., Krzywiec, P., López-Gómez, J., Wetzel, L., et al. (2006). Post-Variscan (end Carboniferous-Early Permian) basin evolution in Western and Central Europe. In D. G. Gee & R. A. Stephenson (Eds.), *European Lithosphere Dynamics* (Vol. 32, pp. 355–388). London: Geological Society Memoirs.

Mundil, R., Brack, P., Meier, M., Rieber, H., & Oberli, F. (1996). High resolution U-Pb dating of Middle Triassic volcaniclastics: Time-scale calibration and verification of tuning parameters for carbonate sedimentation. *Earth and Planetary Science Letters, 141*, 137–151.

Mundil, R., Palfy, J., Renne, P. R., & Brack, P. (2010). The Triassic timescale: new constraints and a review of geochronological data. *Triassic Timescale, 334*, 41–60.

Muttoni, G., Kent, D. V., Garzanti, E., Brack, P., Abrahamsen, N., & Gaetani, M. (2003). Early Permian Pangea 'B' to Late Permian Pangea 'A'. *Earth and Planetary Science Letters, 215*, 379–394.

Nebel, O., Nebel-Jacobsen, Y., Mezger, K., & Berndt, J. (2007). Initial Hf isotope compositions in magmatic zircon from early Proterozoic rocks from the Gawler Craton, Australia: A test for zircon model ages. *Chemical Geology, 241*, 23–37.

Pfiffner, A. (2009). Geologie der Alpen (pp. 359). Göttingen: Haupt Verlag.

Pober, E., & Faupl, P. (1988). The Chemistry of Detrital Chromian Spinels and Its Implications for the Geodynamic Evolution of the Eastern Alps. *Geologische Rundschau, 77*, 641–670.

Robertson, A. H. F. (2006). Sedimentary evidence from the south Mediterranean region (Sicily, Crete, Peloponnese, Evia) used to test alternative models for the regional tectonic setting of Tethys during Late Palaeozoic-Early Mesozoic time. In A. H. F. Robertson & D. Mountrakis (Eds.), *Tectonic Development of the Eastern Mediterranean Region* (pp. 91–154). London: Geological Society Special Publication.

Rottura, A., Bargossi, G. M., Caggianelli, A., Del Moro, A., Visona, D., & Tranne, C. A. (1998). Origin and significance of the Permian high-K calc-alkaline magmatism in the central-eastern Southern Alps, Italy. *Lithos, 45*, 329–348.

Salters, V. J. M., & Stracke, A. (2004). Composition of the depleted mantle. *Geochemistry, Geophysics, Geosystems, 5*, 1–27.

Schaltegger, U., & Gebauer, D. (1999). Pre-Alpine geochronology of the Central, Western and Southern Alps. *Schweizerische Mineralogische und Petrographische Mitteilungen, 79*, 79–87.

Schaltegger, U., & Brack, P. (2007). Crustal-scale magmatic systems during intracontinental strike-slip tectonics: U, Pb and Hf isotopic constraints from Permian magmatic rocks of the Southern Alps. *International Journal of Earth Sciences, 96*, 1131–1151.

Schaltegger, U., Schmitt, A. K., & Horstwood, M. S. A. (2015). U-Th-Pb zircon geochronology by ID-TIMS, SIMS, and laser ablation ICP-MS: Recipes, interpretations, and opportunities. *Chemical Geology, 402*, 89–110.

Scherer, E., Munker, C., & Mezger, K. (2001). Calibration of the lutetium-hafnium clock. *Science, 293*, 683–687.

Schettino, A., & Turco, E. (2009). Breakup of Pangaea and plate kinematics of the central Atlantic and Atlas regions. *Geophysical Journal International, 178*, 1078–1097.

Schettino, A., & Turco, E. (2011). Tectonic history of the western Tethys since the Late Triassic. *Geological Society of America Bulletin, 123*, 89–105.

Schmid, S. M., Fugenschuh, B., Kissling, E., & Schuster, R. (2004). Tectonic map and overall architecture of the Alpine orogen. *Eclogae Geologicae Helvetiae, 97*, 93–117.

Schulz, B. (2008). Basement of the Alps. In T. McCann (Ed.), *The Geology of Central Europe: Precambrian and Palaeozoic* (Vol. 1, pp. 79–83). London: The Geological Society.

Sláma, J., Kosler, J., Condon, D. J., Crowley, J. L., Gerdes, A., Hanchar, J. M., et al. (2008). Plesovice zircon—a new natural reference material for U-Pb and Hf isotopic microanalysis. *Chemical Geology, 249*, 1–35.

Söderlund, U., Patchett, J. P., Vervoort, J. D., & Isachsen, C. E. (2004). The Lu-176 decay constant determined by Lu-Hf and U-Pb isotope systematics of Precambrian mafic intrusions. *Earth and Planetary Science Letters, 219*, 311–324.

Spalla, M. I., & Gosso, G. (2002). Permian-Triassic magmatism and the tectonothermal evolution of the Austroalpine and South-Alpine lithosphere. *Memoir di Scienze Geologiche Padova, 54*, 105–108.

Stampfli, G. M., & Borel, G. D. (2002). A plate tectonic model for the Paleozoic and Mesozoic constrained by dynamic plate boundaries and restored synthetic oceanic isochrons. *Earth and Planetary Science Letters, 196*, 17–33.

Stampfli, G. M., Borel, G. D., Marchant, R. & Mosar, J. (2002). Western Alps geological constraints on western Tethyan reconstructions. In G. Rosenbaum & G. S. Lister (Eds.), Reconstruction of the evolution of the Alpine-Himalayan Orogen. *Journal of the Virtual Explorer* (Vol. 7, pp. 75–104).

Stampfli, G. M., & Kozur, H. W. (2006). Europe from the Variscan to the Alpine cycles. *European Lithosphere Dynamics, 32*, 57–82.

Stampfli, G. M., Hochard, C., Verard, C., Wilhem, C., & vonRaumer, J. (2013). The formation of Pangea. *Tectonophysics, 593*, 1–19.

Stille, P., & Steiger, R. H. (1991). Hf Isotope Systematics in Granitoids from the Central and Southern Alps. *Contributions to Mineralogy and Petrology, 107*, 273–278.

Stockar, R., Baumgartner, P. O., & Condon, D. (2012). Integrated Ladinian bio-chronostratigraphy and geochrononology of Monte San Giorgio (Southern Alps, Switzerland). *Swiss Journal of Geosciences, 105*, 85–108.

Traversa, G., Ronca, S., Del Moro, A., Pasquali, C., Buraglini, N., & Barabino, G. (2003). Late to post-Hercynian dyke activity in the Sardinia-Corsica Domain: A transition from orogenic calc-alkaline to anorogenic alkaline magmatism. *Bollettino Della Societa Geologica Italiana Volume Speciale, 2*, 131–152.

Trevena, A. S., & Nash, W. P. (1979). Chemistry and Provenance of Detrital Plagioclase. *Geology, 7*, 475–478.

Trevena, A. S., & Nash, W. P. (1981). An electron micro-probe study of Detrital Feldspar. *Journal of Sedimentary Petrology, 51*, 137–150.

von Quadt, A., Grünenfelder, M., & Buchi, H. (1994). U-Pb Zircon ages from igneous rocks of the Bernina Nappe System (Grisons, Switzerland). *Schweizerische Mineralogische und Petrographische Mitteilungen, 74*, 373–382.

von Raumer, J. F., Stampfli, G. A., & Bussy, F. (2003). Gondwana-derived microcontinents—the constituents of the Variscan and Alpine collisional orogens. *Tectonophysics, 365*, 7–22.

von Raumer, J. F., Bussy, F., Schaltegger, U., Schulz, B., & Stampfli, G. M. (2013). Pre-Mesozoic Alpine basements-their place in the European Paleozoic framework. *Geological Society of America Bulletin, 125*, 89–108.

Zanetti, A., Mazzucchelli, M., Sinigoi, S., Giovanardi, T., Peressini, G., & Fanning, M. (2013). SHRIMP U-Pb Zircon Triassic intrusion age of the Finero Mafic Complex (Ivrea–Verbano Zone, Western Alps) and its geodynamic implications. *Journal of Petrology, 54*, 2235–2265.